Structural Identification of Doped Silicon Clusters

Yejun Li, André Fielicke, Peter Lievens and Ewald Janssens

Abstract In this chapter we review recent research on the structural identification of isolated doped silicon clusters by combining state-of-the-art experiments and computational modelling using the density functional theory formalism. The experimental techniques include chemical probe mass spectrometric methods, infrared action spectroscopy, photoelectron spectroscopy, and x-ray absorption spectroscopy. Coinage metal elements, transition metals with an incomplete *d* sub-shell, lanthanides, and non-metallic main-group elements are considered as dopant atoms. The growth mechanisms of the doped silicon clusters are described with particular emphasis on the formation of endohedral cages. Specific species that may be considered as building blocks in future nano-structured materials and devices are highlighted, thereby exploiting their unique structural, electronic, or magnetic properties.

Keywords Silicon clusters · Growth mechanism · Dopants in atomic clusters · Molecular beams · Mass spectrometry · Infrared multiple photon dissociation spectroscopy · Photoelectron-spectroscopy · X-ray absorption spectroscopy

Y. Li · P. Lievens · E. Janssens (✉)
Laboratory of Solid State Physics and Magnetism, KU Leuven,
Celestijnenlaan 200d, Leuven 3001, Belgium
e-mail: ewald.janssens@kuleuven.be

Y. Li
e-mail: liyejun-mse@163.com

A. Fielicke
Institut für Optik und Atomare Physik, Technische Universität Berlin,
Hardenbergstrasse 36, 10623 Berlin, Germany

M.T. Nguyen and B. Kiran (eds.), *Clusters*, Challenges
and Advances in Computational Chemistry and Physics 23,
DOI 10.1007/978-3-319-48918-6_2

1 Introduction

The experimental study of small silicon clusters started about 30 years ago with the advent of cluster sources [1–3] and was arguably often motivated by the downsizing of silicon based devices. The properties of silicon clusters are, as for many other atomic clusters, known to vary strongly with size and can be very different from bulk. Notable examples are their size dependent structural motives that are dissimilar from pieces of bulk silicon, such as prolate shaped cationic silicon clusters composed of 20–30 atoms and spherical shapes for larger clusters [4]. Also the photofragmentation behavior of silicon clusters is peculiar with relatively small clusters losing relatively large Si_6 and Si_{10} fragments, as opposed to the more common atom-by-atom evaporation for other types of clusters such as metals [1, 5]. Unlike the isolobal carbon that forms sp^2 hybridized fullerenes and carbon nanotubes, silicon favors sp^3 hybridization [6], which leads to rather asymmetric and reactive structures for pure silicon clusters.

It was shown in the last decades that doping can be used to modify and optimize the structural, electronic, chemical, and magnetic properties of silicon clusters [7, 8]. In particular, doping with transition metals can induce the formation of stable and unreactive cages of high symmetry, which may have appealing properties [9–13]. Following the first experimental realization of transition metal *(TM)* doped silicon clusters and the mass spectrometric discovery of the particular stability of $Si_{15}TM^+$ and $Si_{16}TM^+$ (*TM* = Cr, Mo, W) clusters by Beck [14], a large number of theoretical and experimental studies have been devoted to the structures and properties of endohedrally doped silicon clusters. Famous examples include the predictions of icosahedral $Si_{20}Zr$ [9], hexagonal prism structures for $Si_{12}W$ [10] and $Si_{12}Cr$ [15], fullerene-like $Si_{16}Zr$ [11], Frank-Kasper polyhedral $Si_{16}Ti$ [11], and cubic Si_8Be [16]. These results opened prospects for the production in large quantities of size selected silicon clusters with tailored properties, what is of utmost relevance for the use of silicon clusters as building blocks in future nanostructured devices.

The interest in doped silicon clusters has been so high that almost every element of the periodic table has been considered for doping. Nonetheless, identification of the geometric and electronic structures of doped, and even of bare, silicon clusters still is a great challenge for spectroscopic and theoretical studies alike. For example, it took many years before a consensus was reached on the geometry of Si_6 [17–19] and the lowest energy structure of Si_8^+ was only recently identified [20].

The reason why a dopant can stabilize a high-symmetry silicon cage is still subject of debate. Arguments either refer to bonding between the valence orbitals of the dopant with the silicon cage [9, 21] or to closed electronic shell structures [22] and compact geometries. Electron counting rules were also applied to explain the magic numbers of silicon clusters doped with transition metals. For example, $Si_{12}Cr$ and $Si_{16}Ti$ were claimed to be more stable than their neighboring sizes because of a 18 and 20 electron shell closure, respectively [13, 15]. On the other hand the enhanced stability of $Si_{16}Ti$ also could be explained by bonding arguments with a

combination of 3*d* electrons of the Ti with electrons of the Si cages forming a bonding orbital at the HOMO level of the cluster [23].

In spite of intensive efforts, the influence of different dopants on the structures of the host silicon clusters, in particular on the growth mechanisms that govern the evolution of their physical and chemical properties, is still poorly understood. As a matter of fact, both experiment and theory have been facing difficulties and challenges to investigate the structures of clusters. Computationally, many energetically low-lying isomers may exist for a given cluster size, with small energy differences that are within the accuracy of contemporary methods, in particular for density functional theory (DFT). Hence, it is clear that theory alone does not suffice to accurately predict the most stable geometry of a cluster. Concurrently, experimental studies of clusters in gas phase are far from trivial and there is no single experimental method that straightforwardly probes the geometry and electronic structure of clusters. Chemical probe techniques based on mass spectrometry have been developed and various molecules (H_2O, O_2) or atoms (H, Ar) have been used to probe the transition from exohedral, where the dopant is exposed on the surface of the silicon cluster, to endohedrally doped silicon clusters, where the dopant resides inside a silicon cage [10, 24–26]. These techniques, however, do not provide detailed structural information of the clusters. In the last years, infrared (IR) spectroscopy has proven to be an invaluable technique to determine the structure of clusters in the gas phase, since it is very sensitive to the cluster's internal structure with molecular vibrations reflecting the arrangements of the atoms [27]. The growth patterns of several neutral and cationic transition metal, coinage metal, and non-metal main-group doped silicon clusters have been identified by IR action spectroscopy in combination with DFT calculations [28–33]. Photoelectron spectroscopy (PES) has commonly been used to study the electronic structure of anionic doped silicon clusters, yielding information about electron detachment energies, and in combination with DFT was also used for structural identification [24]. Extensive research efforts by PES were undertaken on transition metal and lanthanide metal atom doped silicon clusters [13, 34–40]. PES probes the electronic signature of valence electrons, which is done in the visible or ultraviolet spectral range and can be performed by standard laboratory lasers. To access the deeper valence bands or core levels, photon energies in the extreme ultraviolet to soft x-ray range are needed, requiring synchrotron radiation facilities or free-electron lasers as light sources. X-ray absorption (XAS) and x-ray magnetic circular dichroism (XMCD) spectroscopy, concentrating on the $2p \rightarrow 3d$ excitation energies of 3*d* transition metal dopants, were used to study the electronic and magnetic properties of doped cationic silicon clusters [26]. XMCD for instance revealed a coordination-driven magnetic-to-nonmagnetic transition in manganese doped Si_nMn^+ clusters [26].

The current chapter focuses on the evolution of geometric and electronic structures of doped silicon clusters as obtained by state-of-the-art experiments in combination with DFT calculations. In view of the extensive amount of literature, we mainly concentrate on recent studies dealing with coinage metal, transition metals with open atomic *d* sub-shells, lanthanides, and non-metallic main-group

elements as dopants. It should be mentioned that there also are plenty of studies on silicon clusters doped with alkali atoms and other main group elements [16, 41–48], which are out of the scope of the present review.

The experimental techniques that have extensively been applied for the structural study of doped silicon clusters in the gas phase are briefly introduced in Sect. 2 with comments on the strengths and limitations of each technique. In Sect. 3, the effects of the different dopants on the growth pattern are discussed on the basis of recent experimental and theoretical results. Also the electronic and magnetic properties of the selected clusters are commented on. Conclusions and an outlook for future work are presented in the final Sect. 4.

2 Experimental Techniques to Study Doped Si Clusters in the Gas Phase

2.1 Mass Spectrometric Techniques

The first reported experimental investigation of doped silicon clusters is a mass spectrometric study of transition metal doped silicon clusters by Beck [14]. After, strikingly high abundances were observed for $Si_{15}TM^+$ and $Si_{16}TM^+$ with *TM* = Cr, Mo, and W, while most other sizes had low abundances. These mass spectra thus revealed the particular stability of certain doped silicon clusters. Beck suggested that the transition metal atom acts as a seed and silicon atoms form a shell around the metal dopant. The work of Hiura et al. constitutes another landmark in the investigation of doped silicon clusters [10]. $Si_nTMH_x^+$ species were produced in an ion trap via the reaction of 5*d* transition metal ions with silane SiH_4 gas [10]. For long ion trapping times, surprisingly the end products are dehydrogenated doped silicon clusters with a maximal size *n* that depends on the transition metal ion. More specifically, for TM^+ with *TM* = Hf, Ta, W, Re, and Ir, the end products were dehydrogenated Si_nTM^+ clusters with *n* = 14, 13, 12, 11, and 9, respectively. It was predicted that those clusters have endohedral structures with the metal ion stabilizing a Si polyhedral cage, indeed confirmed by ab initio calculations for $Si_{12}W$ [10].

Later, mass spectrometric investigations of Cr, Mn, Cu, and Zn doped silicon clusters by Neukermans et al. demonstrated the enhanced stability of $Si_{15,16}Cr^+$, $Si_{15,16}Mn^+$ and $Si_{10}Cu^+$ [49] relative to neighboring sizes. Ohara et al. studied anionic silicon clusters doped with single Ti, Hf, Mo, and W atoms [35]. Also in that work, predominant formation of doped clusters containing 15 and 16 silicon atoms was found independent of the dopant atom, pointing to a geometric stabilization. To better understand the role of the number of valence electrons for the stability of the clusters, a systematical investigation of cationic, neutral, and anionic $Si_nTM^{+/0/-}$ (*TM* = Sc, Y, Lu, Ti, Zr, Hf, V, Nb, and Ta) was conducted by Nakajima and coworkers [13, 34, 50]. Particular enhanced intensities were detected

for the isoelectronic $Si_{16}Sc^-$, $Si_{16}Ti^0$, and $Si_{16}V^+$ species [13]. It was conjectured that these clusters have closed electronic shell structures with 20 itinerant electrons: four from the dopant 3*d* orbitals and one electron from each $3p_z$ orbital of the sp^2-hybridized silicon atoms that are arranged in a caged structure.

While intensities in mass spectrometric studies are useful to obtain information about relative stabilities of certain cluster sizes, the combination of chemical probes with mass spectrometry can provide additional information about the position of the dopant atom. Nakajima and coworkers demonstrated that an exohedral transition metal dopant atom is a reactive site for water [24, 34, 35, 50]. Large doped Si clusters, that presumably adopt a caged structure, show a low reactivity upon exposure to H_2O, while exohedrally doped clusters readily interact with water. Their studies of transition metal doped Si_nTM (*TM* = Sc, Ti, V, Y, Zr, Nb, Mo, Hf, Ta, and W) and lanthanide doped Si_nLn (*Ln* = Tb, Ho, and Lu) clusters provided element and charge state dependent threshold sizes for the reaction with water vapor. Similarly, Lau and coworkers observed a size dependent depletion of singly doped Si_nMn^+ (n = 7–14) in the presence of oxygen, which indicated the exohedral to endohedral transition at n = 10 [26].

Janssens et al. proved that not only the reactivity with molecules such as H_2O, but also the physisorption of argon atoms, can be used as a structural probe for endohedral doping [25]. At 80 K, argon does not attach to elemental silicon clusters but only to surface-located transition-metal atoms. Critical sizes for Ar attachment were found to depend on the size of the transition metal dopant atoms for Si_nTM^+ with *TM* = Ti, V, Cr, Mn, Co, and Cu [25, 51]. As illustrated in Fig. 1, no or negligible Ar physisorption is observed for sizes larger than $Si_{12}Ti^+$, $Si_{11}V^+$, $Si_{10}Cr^+$, $Si_{10}Mn^+$, Si_7Co^+, and $Si_{11}Cu^+$. Agreement with theoretical predictions confirms that these critical sizes for Ar adsorption are indeed related to the formation of endohedral clusters [25]. Furthermore, also doubly doped $Si_nTM_2^+$ clusters show a critical size for Ar adsorption, which might indicate that larger endohedral caged molecules are formed, eventually to be considered as seeds for the growth of metal-doped silicon nanorods [52, 53].

It is obvious that these mass spectrometric techniques alone cannot provide detailed structural information. For example, Ar tagging experiments can hint towards cage formation of Si_nV^+ from n = 11 onwards but cannot differentiate between trigonal and hexagonal prism based structures [28]. More detailed structural and electronic information of doped silicon clusters could be obtained by infrared spectroscopy, photoelectron spectroscopy, or x-ray spectroscopy, as is described in the subsequent sections.

2.2 *Infrared Spectroscopy*

IR spectroscopy is a powerful technique to determine the structure of clusters. The vibrational modes of a cluster, with energies corresponding to far-IR photons, are very sensitive to forces between the atoms and to the structural arrangement of

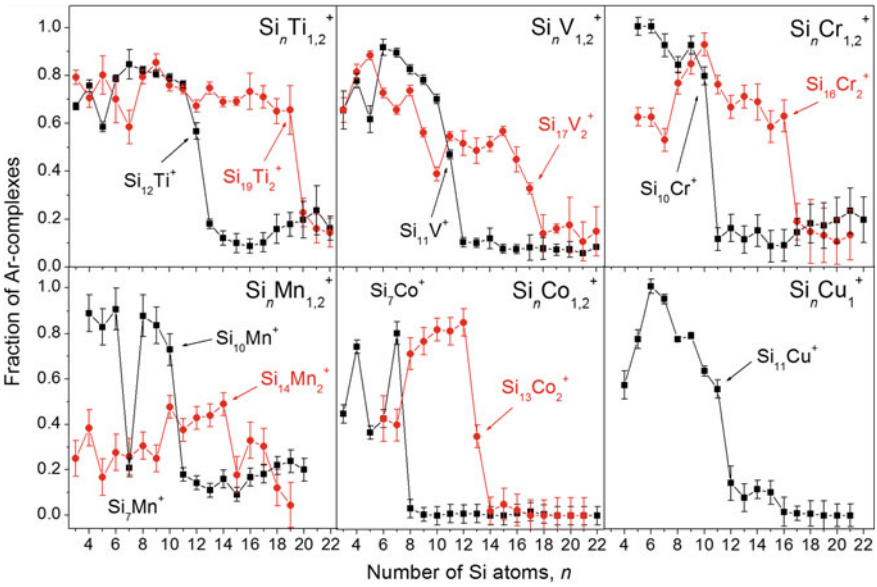

Fig. 1 Fraction of argon complexes formed for $Si_nTM_{1,2}^+$ (*TM* = Ti, V, Cr, Mn, Co, Cu) as function of the cluster size. A dopant dependent critical size, beyond which the argon-complex formation is unlikely, is found for both the singly and doubly *TM* doped species. The critical size likely corresponds to the onset of cage formation. The absence of Ar attachment on Si_7Mn^+ is not caused by encapsulation of the Mn dopant atom but to a very weak interaction between Mn and Ar in Si_7Mn^+•Ar, which is related to a particular electronic shielding effect of the dopant *s*-electrons at this size as discussed in detail in [51]

atoms in a cluster. Conventional IR spectroscopy measures absorption spectra via the wavelength dependence of the transmittance. For sensitivity reasons it is required that a sufficient amount of material is sampled, which makes the technique inappropriate for low-density media such as clusters in the gas phase. In addition, convential IR spectroscopy is not size selective and the spectra of different species in the molecular beam cannot be disentangled, unless prior size selection is made (remark that a cluster source produces a distribution of sizes and compositions). Both mass selectivity and high sensitivity can be obtained by combining IR excitation with mass spectrometry. The reaction of a cluster in reponse to photon absorption is then detected mass spectrometrically in so-called action spectroscopy. Such action can be either a change of mass, cluster dissociation, or a change in its charge state, cluster ionization. The last years basically four experimental techniques for IR action spectroscopy on clusters in the gas phase have been developed (see Fig. 2): IR resonance enhanced multiple photon ionization (IR-REMPI), IR multiple photon dissociation (IR-MPD), infrared-ultraviolet two-color ionization (IR-UV2CI) , and IR multiple photon dissociation spectroscopy of cluster–rare gas complexes [54]. These techniques have in common that a vibrational spectrum is obtained by recording a mass-selective ion yield as a function of the IR radiation

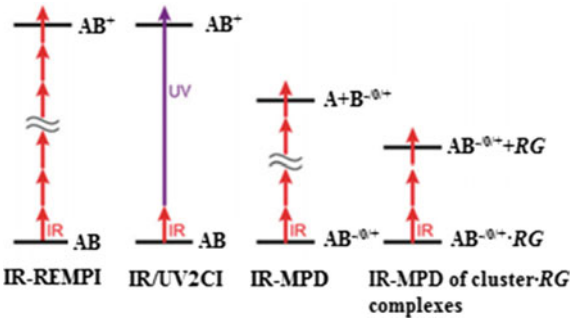

Fig. 2 Schematic presentation of four experimental approaches for IR action spectroscopy of atomic clusters, AB, in the gas phase: IR resonance enhanced multiple photon ionization (IR-REMPI), IR/UV two-color ionization (IR-UV2CI), IR multiple photon dissociation (IR-MPD), and IR multiple photon dissociation of cluster–rare gas complexes. The first two techniques are used for neutral clusters. The last two can be applied both on charged and neutral clusters. In the case of neutral clusters postionization is needed. (Adapted from Asmis et al. (2012) Phys Chem Phys Chem 14:9270)

wavelength and that they require an intense and tunable IR laser source. Of these four techniques IR-UV2CI and IR-MPD of cluster—rare gas complexes have been used to characterize neutral and cationic doped silicon clusters. Those experiments on doped silicon clusters were all done at the Free Electron Laser for Infrared eXperiments (FELIX), Nieuwegein, the Netherlands. Recently this facility was moved to the Radboud University Nijmegen [55].

Silicon clusters are strongly bound with typical bond energies of 2–4 eV [56], while the vibrational transitions of these clusters are typically in the 50–500 cm^{-1} range, corresponding to photon energies of 6–60 meV. Many IR photons are required to dissociate pure and doped silicon clusters, which means the action spectroscopy will not be a coherent multiphoton process. Intramolecular vibrational redistribution of energy is taking place in between successive photon absorption event. Also, given the low absorption probability, even with the available high intensity free electron laser sources, dissociation of silicon clusters is challenging. The so-called messenger atom technique, where weakly bound cluster—ligand complexes are probed instead of pure clusters, can overcome the need of many photons [57, 58]. Such a ligand is typically an inert gas atom, which can be attached to the silicon clusters by adding a small fraction of the messenger gas to the carrier gas in the cluster source and cooling the source to cryogenic temperatures. The loosely bound ligands are supposed to have a negligible influence on the geometry of the clusters. This assumption has to be confirmed ex post and does not always hold [59]. Following absorption of a few IR photons the cluster—rare gas atom bond will break. The light absorption can then be monitored mass spectrometrically by depletion of the complex or alternatively by the increase of the bare cluster abundance.

Structural identification of the clusters can subsequently be obtained by comparison of the experimental IR spectra with computed spectra for different structural isomers. DFT calculations have been the most used computational tool for doped silicon clusters. An example is shown in Fig. 3 for Si_nAu^+ clusters, where the comparison of the experimental and the calculated spectra of the obtained lowest energy isomers for $n = 4, 6, 8, 9, 11$ is depicted [31]. The experimental action spectra were obtained by IR-MPD of Si_nAu^+•Ar or Xe complexes, while DFT calculations were employed using the BP86 functional in combination with the SVP basis set for the Si atoms and the SDD pseudopotential for Au. The rare gas ligand was not included in the computations. The observation that the experimental spectra are well reproduced by the calculations, even for the small features, thus confirms the minor influence of the messenger atom on the cluster's vibrational spectrum in this case. The structures are found to be planar for Si_4Au^+ and three-dimensional for larger sizes. Si_6Au^+ is a distorted octahedron, while Si_8Au^+ and Si_9Au^+ have edge-capped pentagonal bipyramidal structures [31]. However, it should be noted that the structural assignment is not always straightforward. On one hand, the anharmonicity of the potential energy and finite temperature effects are normally not taken into account in the calculations, which will result in band shifts and can have a significant effect on the intensities of bands. On the other hand, DFT calculations have difficulties to properly describe the cluster—rare gas bond. Furthermore, recent kinetic Monte Carlo simulations also demonstrated that the multiple photon character of the action spectroscopy influences the exact frequency, intensity, and width of the adsorption modes [60]. Therefore, a perfect match between theory and experiment cannot be expected. Definite assignments are even more challenging for larger-sized clusters, mainly due to the emergence of many low energy isomers, of which several may have harmonic IR spectra in reasonable correspondence with the experiment. This is illustrated in Fig. 3 for $Si_{11}Au^+$, which has two isomers, with a relative energy of less than 0.2 eV with respect to the obtained ground state. All three could exist in the molecular beam as the main features in their IR spectra show a reasonable agreement with the experimental action spectrum.

The messenger atom technique is not restricted to ionic species only [29]. If the clusters are postionized by a single photon with an energy above the cluster's ionization potential, IR spectroscopy of neutral cluster—rare gas complexes can be done in an analogous way as for ionic species. This was illustrated by Claes et al. for small neutral Si_nV and Si_nMn ($n = 6–9$) clusters tagged with Xe [29].

The inherent disadvantage of the messenger atom techniques is the possible perturbation of the cluster's structure by the adsorbed ligand, even if weakly bound rare gas atoms are used. Also in specific cases, especially for neutral clusters, it is quite difficult to create cluster—rare gas complexes, even at low temperatures. An alternative method for neutral clusters, without the need for formation of messenger atom complexes, is the IR-UV2CI technique [17, 61]. This generally applicable technique combines IR excitation with near threshold photoionization. It relies on the absorption of a single (or a few) IR photons prior to absorption of a UV photon, which has a photon energy just below the ionization energy, to lift the total internal

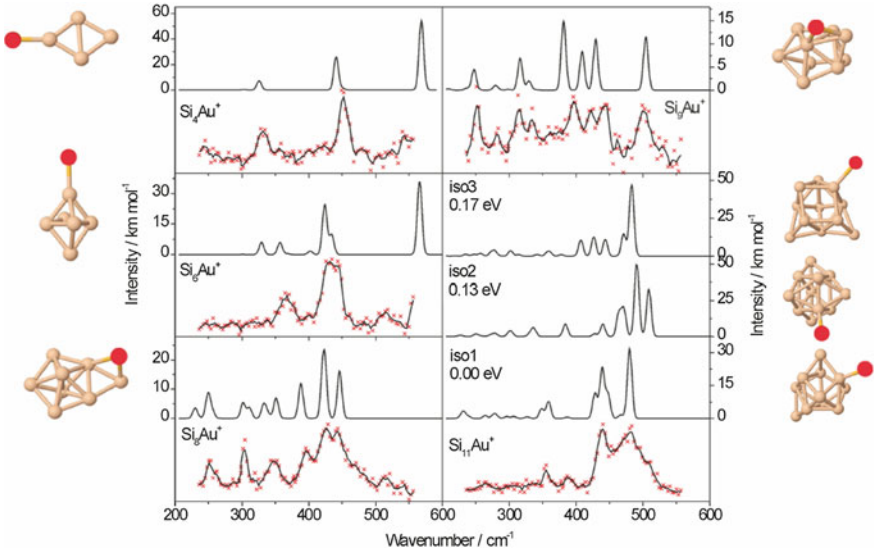

Fig. 3 Experimental IR-MPD spectra (*lower traces*) of Si_nAu^+·Ar (n = 4, 6, 9) and Si_nAu^+·Xe (n = 8, 11), the calculated harmonic single photon adsorption spectra (*full lines*, traces above the experimental data), and the geometric structures (*left* and *right*) of the obtained lowest-energy isomers. The *crosses* are the original data points, while the *full lines* correspond to three-point running averages

energy of the species above the ionization threshold. The direct photoionization generally prevails over the slower statistical fragmentation process. The formed ions can be sensitively detected by means of mass spectrometry. Scanning the energy of the IR photons changes the ionization efficiency and the recorded ion intensity reflects the IR absorption spectrum of the corresponding neutral clusters. This is illustrated by the mass spectrum in Fig. 4 for Si_nCo clusters. Species with a vertical ionization energy close to (or slightly above) the photon energy of the ionization laser (such as Si_nCo with n = 10–12) have a low intensity in the mass spectra (Fig. 4a), but show enhanced abundance if they are excited by resonant absorption of one or more IR photons prior to interaction with UV radiation (Fig. 4b). By comparison of the IR-UV2CI spectra of Si_nCo (n = 10–12) with simulated IR spectra for different structural isomers (not shown), endohedral geometries were assigned to those clusters [61].

2.3 Photoelectron Spectroscopy

PES is a commonly used technique to study the electronic structures and chemical bonding of gas-phase atomic clusters. The basic physical idea behind PES is simple: a cluster is excited by absorption of a single photon with a photon energy

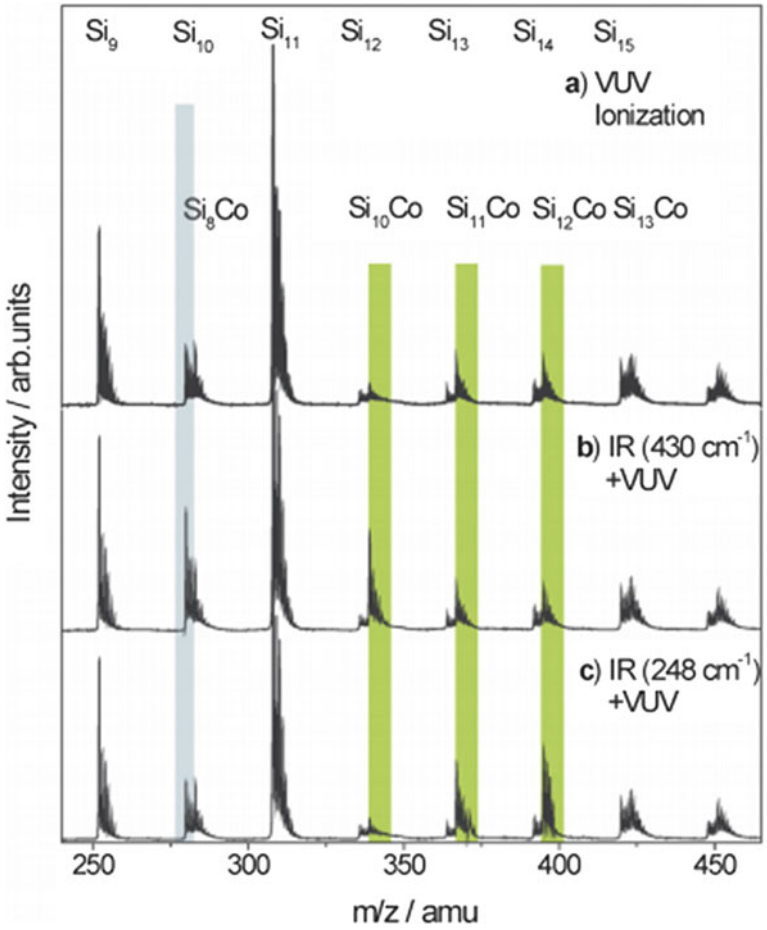

Fig. 4 Mass spectra of neutral Si_n (n = 9–16) and Si_nCo (n = 7–14) clusters obtained under different ionization conditions. **a** Mass spectrum obtained by ionization with 7.87 eV UV photons solely. **b** Prior irradiation of the neutral cluster distribution with intense IR light at 430 cm^{-1} significantly increases the signal of Si_{10} and $Si_{10}Co$, while the rest of the mass spectrum is nearly unchanged. **c** Irradiation with IR light of 248 cm^{-1} followed by UV ionization enhances the intensities of $Si_{11}Co$ and $Si_{12}Co$. (Reproduced from Li Y et al. (2014) J Phys Chem A 37:8198)

exceeding the binding energy of the least bound electron, which results in electron detachment. The remaining part of the incoming photon energy is shared by the ionized cluster and the photoelectron. Since the mass of the cluster is much larger than that of the electron, most excess energy is converted into kinetic energy of the emitted electron. Hence, measuring the intensity of photoelectrons as a function of their kinetic energy provides a spectrum of the occupied electronic energy levels of the cluster.

PES is usually performed on anionic clusters, since the charge is required for size selection and anions usually have low valence electron binding energies that are accessible by commercial lasers, such as the 2nd, 3rd or 4th harmonics of a Nd:YAG laser. An anion photoelectron spectrum provides the adiabatic detachment energy (ADE) and the vertical detachment energy (VDE), as well as the electronic excitation energies, which constitute an electronic fingerprint of the cluster. PES on anionic clusters also yields information about the corresponding neutral species. Since the detachment process is fast in comparison to structural arrangement of the nuclei upon removal of the electron, anion photoelectron spectroscopy probes the electronic structure of a neutral cluster in the ground state geometry of its anion. The resulting neutral cluster can hereby either be in the vibronic ground state or in a vibronically excited state. For example the adiabatic electron affinity (EA_a) of Si_nEu (n = 3–17) clusters was inferred from their photoelectron spectra [37]. For small sizes n = 3–11 the EA_a is relatively small and ranges from 1.45–2.2 eV. However, it shows an abrupt increase (EA_a > 2.5 eV) from n = 12 onwards, which has been related to geometric rearrangements from exohedral to endohedral structures [37].

In addition to the valuable knowledge about the electronic states, PES can be used for structural assignment if changes in the geometry lead to changes in the electronic levels. The photoelectron spectrum of various isomers can be simulated by means of quantum chemical calculations if the generalized Koopman's theorem is applied to predict vertical detachment energies of different occupied orbitals. The cluster structure can then be assigned through comparison of the PES spectrum with simulated density of states (DOS) of candidate isomeric structures.

Figure 5 depicts the photoelectron spectra of $Si_{12}V_n^-$ (n = 1, 2, 3) clusters as recorded by Zheng and coworkers using the 4th harmonic (4.66 eV) of a Nd:YAG laser [38]. The photoelectrons are energy-analyzed by a magnetic bottle photoelectron spectrometer. The experimental photoelectron spectra of $Si_{12}V_n^-$ are well reproduced by DFT computations applying the generalized Koopman's theorem. With the structures identified, the computations of the electronic structures were used to infer other physical properties. It was found that $Si_{12}V_3^-$ shows a total spin of 4 μ_B with a ferromagnetic coupling between the V dopants, while $Si_{12}V^-$ and $Si_{12}V_2^-$ favor low spin states.

2.4 *X-Ray Absorption and Magnetic Circular Dichroism Spectroscopy*

While the valence electron spectra of size-selected anionic clusters can be obtained by PES using commercial laser systems in the visible or UV spectral range, access to deeper core electron levels requires photon energies in the extreme ultraviolet to soft X-ray range. X-ray absorption experiments can be performed at synchrotrons and provide element specific electronic and magnetic information, which is particularly valuable for the study of doped clusters. They are, however, challenging

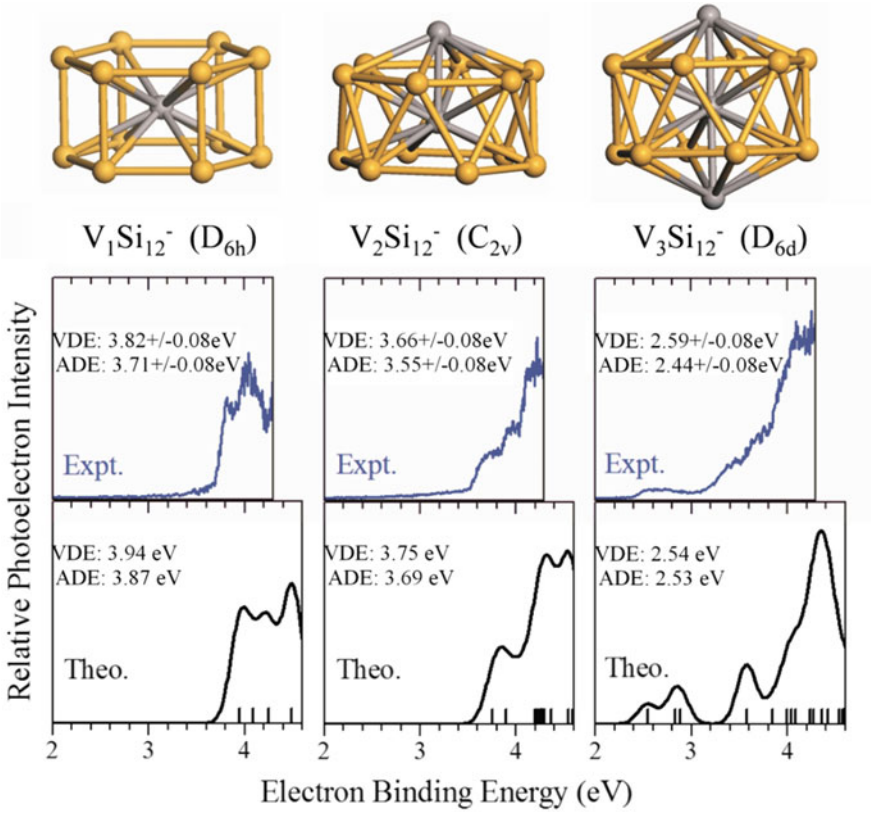

Fig. 5 Photoelectron spectra of $Si_{12}V_m^-$ (m = 1, 2, 3) clusters. *Upper* geometrical structures; *middle* experiment; *lower* theoretical simulation using DFT and a uniform Gaussian broadening of 0.1 eV for each vertical detachment process. The individual calculated energy levels are labelled by *short vertical lines*. Both the measured VDE and ADE are well reproduced by the simulated values for the obtained lowest energy isomers. (Adapted from Huang X et al. (2014) Nanoscale 6:14617)

for clusters in the gas phase given the low target density and the required high photon fluence [62].

Opposed to PES and IRMPD experiments, which are often done in molecular beams, X-ray experiments on clusters in the gas phase are usually performed in an ion trap to ensure a high density of size selected clusters. Size selected trapped clusters are electronically excited by a collinear beam of tunable soft X-ray radiation and will undergo fragmentation and multiple ionization steps. Ions are subsequently extracted from the ion trap and analyzed in a time-of-flight mass spectrometer. X-ray absorption spectra are obtained by monitoring the yield of cluster fragment ions as a function of incident photon energy. For XMCD spectroscopy low temperatures and high magnetic fields are required to align the magnetic moment of the clusters. This can be done by a superconducting solenoid

in combination with cryogenic cooling of the ion trap and a buffer gas for thermal equilibration of the clusters [26]. Ion yield spectra are then recorded for parallel and antiparallel alignment of the photon helicity and magnetic field.

The basic principle of XAS is the absorption of an X-ray photon by a single atom, exciting a core electron. The excited core electron either goes into an empty valence state (resonant photoabsorption) or, if the photon energy is sufficient, into a continuum state above the ionization energy (non-resonant photoionization). A core hole is created in both cases, making XAS a local and element specific method due to the strong localization of the created core hole and the characteristic binding energy of the core electrons. Moreover, for resonant photoabsorption experiments also valence electron information is obtained. Indeed, because of the dipole selection rule $\Delta l = \pm 1$ one can selectively probe specific orbital angular momentum states of the empty valence electron levels.

Quantitative magnetic information of the clusters can be obtained by XMCD spectroscopy. Hereto the ion trap is placed inside a high magnetic field (for instance provided by a superconducting solenoid), so that their magnetic moments are (partly) aligned. Circularly polarized x-ray radiation is then used to measure the differential X-ray absorption spectra for left- and right- handed circularly polarized X-ray beams. Using magneto-optical sum rules both element specific orbital and spin magnetic moment information can be extracted from the dichroic signal [63]. In this case, the dipole selection rule is expanded with $\Delta m_l = +1$ and $\Delta m_l = -1$ for right and left circularly polarized radiation, respectively. For an unequal occupation of the m_l states, the absorption of right and left circularly polarized light will be different. Note that also magnetic deflection experiments can be used to investigate cluster magnetism, in particular total magnetic moments of neutral clusters. We are, however, not aware of any magnetic deflection experiment on doped silicon clusters.

XAS and XMCD have been used to study transition metal doped silicon clusters by Lau and coworkers [26, 64, 65]. Using XAS the electronic structure of the *TM* dopant in Si_nV^+ (n = 14–18), $Si_{16}Ti^+$, and $Si_{16}Cr^+$ was probed via $2p \rightarrow 3d$ transitions, i.e., at the $L_{2,3}$ edges [64]. Figure 6 shows that $L_{2,3}$ X-ray absorption spectra of $Si_{16}Ti^+$, $Si_{16}V^+$, and $Si_{16}Cr^+$ clusters and those of isolated Ti^+, V^+, and Cr^+ ions. The XAS spectra of the isolated ions (upper panel of Fig. 6) have multiplet electronic structures characteristic for each element, and reflect the different $3d$ orbital occupancies of Ti^+, V^+, and Cr^+. However, these differences disappear in case the corresponding atoms are encapsulated in Si_{16} cages. $Si_{16}Ti^+$, $Si_{16}V^+$, and $Si_{16}Cr^+$ endohedral clusters exhibit a very similar fine structure in their X-ray absorption spectra (lower panel of Fig. 6). The relative excitation energies, both the intense features at 0 and 2.1 eV and the less intense ones at 1.1 and 5.0 eV, are practically identical for the three transition metal doped silicon clusters. These similarities imply nearly identical local electronic states of the transition metal dopant atoms, which further indicates a very similar structural environment, as XAS is very sensitive to both [64].

XMCD was used to study Si_nMn^+ (n = 7–14) via the $L_{2,3}$ local $2p \rightarrow 3d$ excitations of the Mn dopant [26]. A clear correlation of the magnetic moment with the

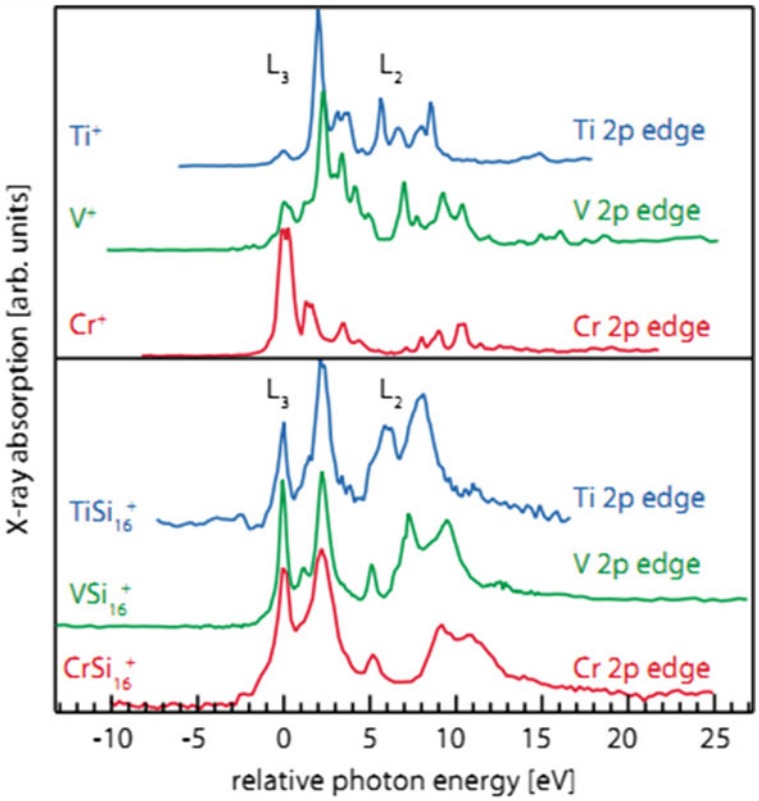

Fig. 6 Transition metal $L_{2,3}$ X-ray absorption spectra of $Si_{16}Ti^+$, $Si_{16}V^+$, and $Si_{16}Cr^+$ clusters (*lower panel*) and of single Ti^+, V^+, and Cr^+ ions (*upper panel*). The spectra are aligned at the first peak position. While the bare ions have different spectra, the relative excitation energies of transition metal dopants in silicon clusters are nearly identical. This surprising fact indicates almost identical local electronic structure at the dopant atom site. Relative positions of the L_2 edge shift because of decreasing $2p$ spin-orbit splitting from chromium to titanium. (Reproduced from Lau JT et al. (2009) Phys Rev A 79:053201)

manganese coordination number and nearest-neighbor distance was found. This work indicated quenching of the Mn magnetic moment at coordination numbers corresponding to those in bulk silicon as a consequence of $3d$ electron delocalization because of the strong interaction between Mn and the silicon cage. The correlation of the magnetic moment and the weighted coordination number provides guidelines to the stabilization of high-spin states in dilute manganese-doped silicon [26].

It was also shown that direct and resonant core-level photoionization spectroscopy in combination with valence band photoionization curves can be used to accurately quantify HOMO–LUMO gaps of size-selected clusters via a Born-Haber cycle [65]. In particular the size-evolution of the HOMO–LUMO gaps of Si_nV^+

(n = 15–17) was obtained by this novel method, confirming the special electronic stability of $Si_{16}V^+$. The method was claimed to be widely applicable and expands the range of current techniques for the determination of band gaps to ultra-dilute samples and electron binding energies in the vacuum UV spectral range.

3 Dopant Dependent Growth Mechanisms and Properties

3.1 Coinage Metal Dopants ($kd^{10}(k + 1)s^1$)

Coinage metal (Cu, Ag, and Au) doped silicon clusters have been studied extensively by DFT calculations. For instance, Xiao et al. showed that the most stable isomers of Si_nCu (n = 4, 6, 8, and 10) have either Si frameworks similar to the structures of the ground state or low-lying isomers of bare Si_n or that Cu is making substitutions in Si_{n+1} [66]. It was also demonstrated that the structure of the Si framework in Si_nCu is largely determined by the Si–Si interactions, because they are stronger than the Si–Cu interactions. However, several computational predictions of the structures of coinage metal doped silicon clusters are in disagreement with one another, especially concerning the dopant induced cage formation. For example, Chuang et al. predicted by first-principles calculations at the PBE/PAW level that Si_nAg clusters (n = 1–13) have exohedral structures with the Ag dopant atom taking a capping position [67], while another computational study (using B3LYP/3-21G*) of Si_nAg (n = 1–15) by Ziella et al. indicated endohedral geometries for $n > 10$ [68]. Conflicting computational predictions were also made for neutral Si_nAu clusters. Wang et al. studied (at B3PW91/LanL2DZ and PW91/DNP levels) the configurations, stability, and electronic structure of neutral Si_nAu (n = 1–16) clusters and found that the Au dopant moves to an interior site in $Si_{11}Au$ and that $Si_{12}Au$ adopts an endohedral structure [69], while Chuang et al. (PBE/PAW) obtained exohedral geometries for neutral Si_nAu (n = 1–16) [70].

The geometry of the coinage metal doped silicon clusters has extensively been investigated by IR-MPD spectroscopy of cluster–rare gas complexes in combination with DFT calculations [30, 31, 33, 71]. The growth mechanisms, assigned on the basis of this combined experimental and computational work, of Si_nCu^+ (n = 2–11), Si_nAg^+ (n = 6–15), and Si_nAu^+ (n = 2–15) clusters are summarized in Fig. 7. In view of the similar electronic structure ($kd^{10}(k + 1)s^1$) of the coinage metal atoms, one may expect that they have a similar influence on the geometry of the silicon clusters. There are indeed similarities in the growth mechanisms of Si_nCu^+, Si_nAg^+, and Si_nAu^+ clusters. It is found that all studied sizes have exohedral structures, in which the dopant atoms favor adsorption on bare Si_n^+ clusters rather than taking substitutional positions as is the case in silicon clusters doped by transition metal elements like V or Mn [32, 33]. This difference must be related to the occupancy of the valence d orbitals. Also the silicon building blocks in Si_nCu^+,

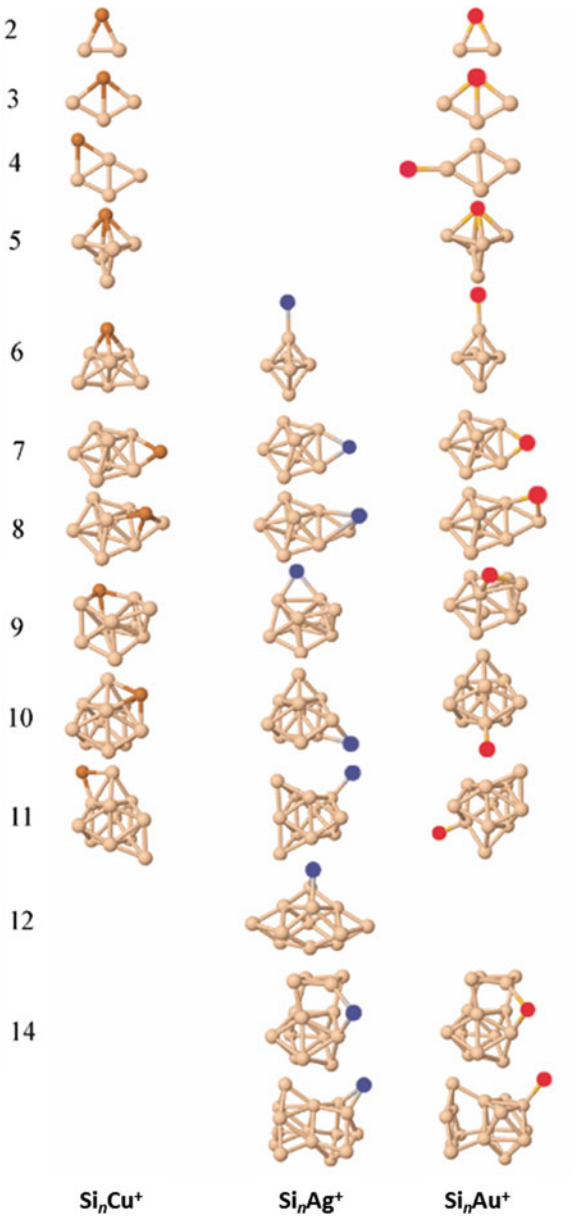

Fig. 7 Structural evolution for Si_nCu^+ (*left*), Si_nAg^+ (*middle*), and Si_nAu^+ clusters (*right*). The structures are assigned based on comparison of IR-MPD spectra, measured on the corresponding cluster—rare gas complexes, with harmonic vibrational spectra calculated for different structural isomers by DFT. (Reproduced from Li Y et al. (2015) J Phys Chem C 119: 10896-10903)

Si_nAg^+, and Si_nAu^+ are similar: the clusters are based on a pentagonal bipyramid for n = 7–9, while a transition to a trigonal prism motif appears from n = 10.

There are, however, also differences between the structures of Cu, Ag, and Au doped silicon clusters. Si_nAg^+ and Si_nAu^+ have similar structures for the smallest sizes (n = 6–8) and for n = 14, while the dopants cap a different position for n = 9

and 10, or the doped clusters adopt different Si frameworks (n = 11 and 15). In general, there seems to be a trend that Cu likes facial, Ag edge, and Au corner positions (see Fig. 7) [31]. It was shown that the d orbital occupancy of the coinage metal dopant plays an important role in the binding site. Natural electron configuration analysis gives that the number of electrons in 4d orbitals of Ag in Si_nAg^+ is slightly higher (9.9) than that in Cu 3d orbitals of Si_nCu^+ (9.8) [30]. Because of this difference in occupancy, Ag prefers to add to the bare Si clusters in a lower coordinated position than Cu. The same may hold for Au in Si_nAu^+ clusters. The coinage metal dopants thus add to the bare Si_n clusters with coordination numbers decreasing from Cu over Ag to Au.

Formation of endohedrally doped cages is experimentally not observed for coinage metal doped silicon clusters, until the largest sizes studied, which is n = 15 for Si_nAg^+ and Si_nAu^+ (see Fig. 7). For Si_nCu^+ the situation is less clear. The IR spectra of cluster–rare gas complexes demonstrated that for $n \leq 11$ no caged structures are formed, but larger sizes were not studied [33]. Larger sizes might be endohedral as predicted computationally [66, 72] and as implied from mass spectrometric experiments, which showed that $Si_{11}Cu^+$ is the critical size for Ar attachment hinting that the Cu dopant atom may take an interior position in larger Si_nCu^+ clusters [25].

The atomic radius of the dopant atom has been shown to play an important role in determining the critical size for cage formation of the transition metal doped silicon clusters [25, 73]. It may also have a significant influence on the binding site of the coinage metal dopant. Au and Ag have similar atomic radii (0.174 and 0.165 nm), which are larger than that of Cu (0.145 nm), therefore, they prefer a more facial (low coordinated) position on the Si clusters and more Si atoms are needed to encapsulate them. The similar growth patterns of Si_nAg^+ and Si_nAu^+, without cage formation up to n = 15, indicate that not only the atomic radius of the dopant atom but also the occupancy of the valence d orbitals and the orbital hybridization between the dopant atom and Si atoms are important in the formation of endohedral structures [74].

Aside from the IR spectroscopy work on cationic coinage metal doped Si clusters, PES investigations were performed on anionic coinage metal doped Si clusters. Zheng and coworkers conducted a combined PES and DFT study on the electronic and geometrical structures of Si_nCu^- (n = 4–18) [75] and Si_nAg^- (n = 6–12) [40]. They tentatively assigned the structures of these clusters based on the comparison between the experimental and calculated photoelectron spectra, vertical detachment energies, and adiabatic detachment energies. It was found that Si_nCu^- ($n > 12$) clusters have endohedral structures. This critical size is consistent with the above mentioned Ar physisorption experiment on cationic Si_nCu^+ clusters [25]. The Si_nAg^- (n = 6–12) clusters are predicted to all have exohedral structures. Most structurally assigned anionic clusters are different from the corresponding cationic Si_nAg^+ and Si_nCu^+ clusters, although they have in common that the Ag dopant seems to take a lower coordinated position than the Cu dopant.

3.2 Transition Metal Dopants (kd^x $0 < x < 10$)

Among all elements in the period table, transition metal atoms and in particular 3*d* transition metal atoms have been used most frequently as dopants in silicon clusters. We therefore do not intend to give an exhaustive overview and concentrate on some recent combined experimental and computational results.

Mass spectrometric Ar tagging experiments predicted that Si_nV^+ adopts endohedral cage structures from $n = 12$ onwards [25]. The geometry of cationic vanadium doped silicon clusters, Si_nV^+ ($n = 4$–16), was investigated in more detail by IR-MPD in combination with DFT calculations [33, 71]. The IR spectra of Si_nV^+ ($n = 4$–11) were measured on the corresponding Si_nV^+•Ar rare gas complexes, which could be formed for the exohedrally doped silicon clusters [33]. Different from coinage metal dopants, the V substitutes a highly coordinated silicon atom of the pure cationic bare silicon clusters. The different growth pattern of Si_nV^+ and Si_nCu^+ clusters reflects the role of the dopant's 3*d* orbital occupancy on the binding. The natural electronic configurations obtained by the natural bond orbital (NBO) method indicated that the number of electrons in the V 3*d* orbitals varied from 3.3 ($n = 6$) to 5.6 ($n = 11$) in Si_nV^+. To probe endohedral Si_nV^+ ($n = 12$–16) clusters by IR-MPD, Xe was used as messenger atom, which does bind to Si due to its higher polarizability than Ar [28]. The assigned Si_nV^+ ($n = 12$–16) clusters have Si frameworks that are significantly different from bare Si clusters. Si_nV^+ ($n = 12$–14) have hexagonal prism based structures, $Si_{15}V^+$ is found to be built up from pentagons and rhombuses, and $Si_{16}V^+$ has a slightly distorted Frank-Kasper polyhedral geometry.

$Si_{16}V^+$ is one of the best studied doped silicon clusters in the literature and was computationally predicted to have a symmetric Frank-Kasper polyhedral structure [12, 23, 76]. Its stability was rationalized by means of an electron counting rule. Each Si atom binds to the V dopant and contributes one delocalized electron to the electron count. With the five valence electrons of V and the cationic state of the cluster, this results in a 20 electron closed shell system [77]. Its broad spectral lines in the IR-MPD experiments were initially suggested to be related to the fluxional behavior of $Si_{16}V^+$ resulting from rapid interchange of the atomic positions between a slightly distorted and a perfect Frank-Kasper polyhedral geometry corresponding to the ground state (**iso1**-T) and a transition state (**TS**-T_d), respectively (see Fig. 8). Molecular dynamics simulations revealed that the Si cage is highly dynamic showing movement and interchange within a quasi-liquid Si shell [28]. The high symmetry of cold $Si_{16}V^+$ was confirmed by Lau et al. through X-ray absorption spectroscopy at the transition metal $L_{2,3}$ edges, which revealed a nearly identical local electronic structure of the dopant atoms in $Si_{16}Ti^+$, $Si_{16}V^+$, and $Si_{16}Cr^+$ in spite of a different number of valence electrons [64]. The HOMO–LUMO gaps of Si_nV^+ ($n = 15$–17), derived by a combination of direct and resonant core-level photoionization spectroscopy with valence band photoionization curves, showed a striking size-dependence and gave further evidence of the special electronic structure and stability of $Si_{16}V^+$ [65].

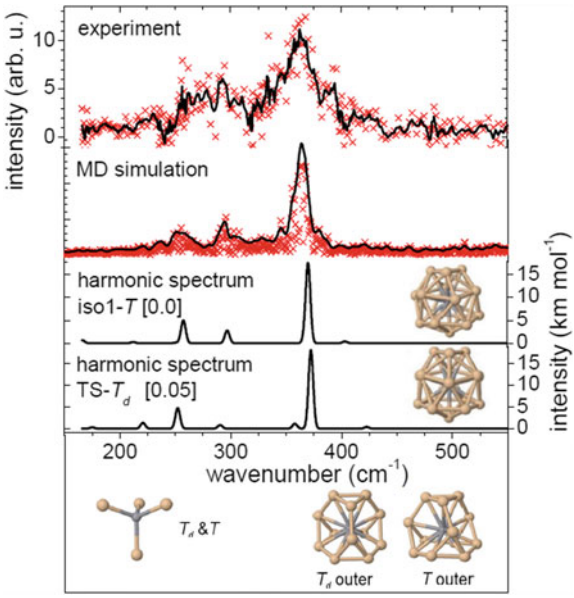

Fig. 8 IR-MPD spectrum of $Si_{16}V^+$•Xe (*upper trace*). The 2nd trace shows the IR spectrum obtained from the molecular dynamics (MD) simulation starting from **iso1**-*T* (*crosses*) and a spectrum that is obtained by overlaying the discrete points with a 5 cm^{-1} FWHM Gaussian profile (*line*). Computed harmonic vibrational spectra of **iso1**-*T* and **TS**-T_d are given in the 3rd and 4th traces. Relative energies in eV at the BP86/6-311 + G(d) level are given in brackets. The structures shown in the *lower trace* represent the *inner* tetrahedral and *outer shells* of **TS**-T_d and **iso1**-*T*. Relaxing from T_d to *T* symmetry, the *inner shell* remains essentially unchanged while the *outer shell* is distorted at the symmetrical planes. The small barrier over **TS**-T_d between degenerate **iso1**-*T* states suggests fluxional rearrangement. The MD simulated trajectory supports the interpretation of $Si_{16}V^+$ undergoing rapid transitions between nearly degenerate local minima. This fluxional behavior leads to a broadening of the IR absorption bands. (Reproduced from Claes P et al. (2011) Phys Rev Lett 107:173401)

Bowen and coworkers measured photoelectron spectra of Si_nCr^- (n = 8–12) following excitation by 355 nm photons [78]. They speculated that the onset of cage formation may be at n = 8. The high VDE found for $Si_{12}Cr^-$ is consistent with the theoretical prediction of an enhanced stability for this cluster [15]. A combined PES and DFT study of anionic Cr doped silicon Si_nCr^- (n = 3–12) refined the earlier prediction and the structural transition from exohedral to endohedral was shown to occur at n = 10 [39]. This critical size is close to the prediction for cationic Si_nCr^+ based on mass spectrometric Ar physisorption experiments, where $Si_{11}Cr^+$ is found as the smallest endohedral Si_nCr^+ cluster (see Fig. 1). Similar to Mn doped silicon clusters, the magnetic properties of Si_nCr^- correlate with their geometric structures. Computations found high magnetic moments (3–5 μ_B) for small (n = 3–9) exohedral structures, while larger (n = 10–12) endohedral sizes have low local magnetic moments (1 μ_B). Also the local charges on the Cr atom

abruptly increase from $n = 10$ onwards. $Si_{12}Cr^-$ was predicted to have a D_{3d} structure with the Cr atom encapsulated in a Si_{12} hexagonal prism cage and enhanced stability [39], in agreement with earlier work [15].

Similar approaches were used to study Si_nMn^+ (n = 6–10, 12–14, and 16) clusters [32]. The Mn dopant favors substitution of a Si atom in Si_{n+1}^+ cations for small, exohedral Si_nMn^+ (n = 6–10), while the endohedral Si_nMn^+ (n = 12–14, and 16) clusters have fullerene-like structures. Opposed to several other 3*d* transition-metal dopants, the Mn dopants in small Si_nMn^+ (n = 6–10) clusters have, according to natural population analysis on the experimentally assigned isomers, high local magnetic moments. The atomic charges on the Mn dopant are around +1 e for all the considered clusters with electron populations of around 0.3 e in the Mn 4*s* and 5.6 e in the Mn 3*d* atomic orbitals. Si_7Mn^+ is a remarkable exception in which both the 4*s* and the 3*d* Mn atomic orbitals are half filled [51]. The electronic and magnetic properties of the Si_nMn^+ (n = 7–14) clusters were analyzed in detail by a combined experimental (XAS and XMCD spectroscopy) and theoretical study [26]. In line with the predictions above, magnetic moment quenching or better a transition from high spin to low spin state was found to coincide with the exohedral to endohedral structural transition around $Si_{11}Mn^+$. The quenching of the magnetic moment is due to the Mn 3*d* electron delocalization because of the strong interaction of the Mn dopant with the silicon cage in case the dopant is highly coordinated.

To investigate the effect of charge on the geometrical and electronic properties of Mn and V doped silicon clusters, a combined experimental and theoretical study was carried out on $Si_nTM^{0/+}$ (TM = V, Mn; n = 6–9) [29]. In general, the effect of the charge state was found to be small. Neutral and cationic $Si_nV^{0/+}$ and $Si_nMn^{0/+}$ clusters have similar geometrical structures, although the positions of the capping atoms are different for some sizes. This similarity is also reflected in the electronic structure with the additional electron in the neutral clusters occupying the majority spin LUMO of the corresponding cation. The analysis of the NBO charge on the transition metal atom showed that most of the additional electron charge in the neutral clusters is distributed over the silicon framework. In contrast, a PES study by Zheng and coworkers [79], in which the most likely structures of these clusters were identified by comparing calculated and experimental VDEs, showed that the structures of anionic Si_nV^- (n = 3–6) clusters are different from their cationic and neutral counterparts.

The structures of cobalt doped neutral silicon clusters, Si_nCo (n = 10–12), were recently investigated by IR-UV2CI experiments [61]. These clusters prefer caged structures in which the silicon frameworks are double-layered. Electronic structure analysis indicated that the clusters are stabilized by an ionic interaction between the Co dopant atom and the silicon cage due to the charge transfer from the silicon valence *sp* orbitals to the cobalt 3*d* orbitals. The DOS revealed a pronounced electronic shell structure. For instance, $Si_{10}Co$ has 49 valence electrons (4 for each Si atom and 9 for Co). By comparison of the molecular orbitals with wave functions of a single free electron in a square well potential with a spherical shape, the level sequence of the occupied electronic states in $Si_{10}Co$ can be described as

$(1S)^2(1P)^6(1\ D_a)^6(1D_b)^4(2S)^2(2\ D_a)^2(1F_a)^2(2D_b)^8\ (1F_b)^6(1F_c)^6(2P)^5$. The subscripts a, b, and c indicate that the degeneracy of the high angular momentum states (1D, 2D, and 1F) is lifted because of crystal field splitting related to the distortion from spherical symmetry of the cluster. The most important difference with the energy level sequence of free electrons in a square well potential is the lowering of the 2D level. Examination of the 2D molecular orbitals shows that they are mainly composed of the Co 3*d* atomic orbitals, representing the strong hybridization between the central Co atom and the surrounding Si cage. In the same study it was also shown that the strong hybridization between the Co dopant atom and the silicon host quenches the local magnetic moment on the encapsulated Co atom [61].

The particular stability of the $Si_{16}TM^+$ clusters was systematically investigated by Nakajima and coworkers using mass spectrometry, anion photoelectron spectroscopy, adsorption reactivity, and theoretical calculations [13, 50]. Enhanced abundances were found for $Si_{16}Sc^-$, $Si_{16}Ti$, $Si_{16}V^+$, $Si_{16}Nb^+$, and $Si_{16}Ta^+$ clusters in addition to high threshold energies for electron detachment, large HOMO–LUMO gaps, and abrupt drops in reactivity towards H_2O adsorption from $n = 16$ onwards. X-ray absorption spectroscopy experiments by Lau et al. predicted highly symmetric silicon cage structures for $Si_{16}Ti^+$, $Si_{16}V^+$, and $Si_{16}Cr^+$ [64], indicating that the interaction with the silicon cage determines the local electronic structure of the dopants, while the dopants induce a geometric rearrangement of the silicon clusters.

Theoretical investigations have been carried out for some other transition metal doped silicon clusters. A review of all theoretical work on transition metal doped silicon clusters is beyond the scope of this chapter, but we will briefly discuss a selection of recent results. A DFT study by Ma et al. has shown that the equilibrium site of the Fe dopants in Si_nFe ($n = 2$–4) gradually moves from convex, over surface, to concave sites as the number of Si atoms increases [74]. From $n = 10$ onwards the Fe atom is at the center of a Si outer frame, forming metal-encapsulated Si cages [74]. For neutral Si_nFe ($n = 1$–8) clusters, Liu et al. predicted trigonal, tetragonal, capped tetragonal, capped pentagonal, and combined tetragonal bipyramids as ground state structures for $n = 4$–8 [80]. Although the located ground states are essentially similar for both neutral and cationic Si_nFe ($n = 1$–8) clusters, the structures of their anionic counterparts are significantly deformed. Endohedral larger neutral Si_nFe ($n \geq 9$) clusters were recently studied by Chauhan et al. [21]. They concluded that the stability of those clusters was determined in the first place by structural arguments such as compact geometries and high symmetric cages, allowing a better mixing of Fe 3d and Si 3p states, rather than by electron counting rules. According to Deng et al., small Si_nTi ($n = 1$–8) clusters have pyramidal structures: trigonal pyramid ($n = 4$), trigonal bipyramid ($n = 5$), square bipyramid ($n = 6$), pentagonal bipyramid ($n = 7, 8$), and they follow a growth pattern where the Si atom prefers to cap $Si_{n-1}Ti$ to form Si_nTi [81]. For Si_nTM ($n = 8$–16) with TM = Ti, Zr, and Hf, Kawamura et al. predicted basketlike structures for $n = 8$–12 and endohedral structures for $n = 13$–16 [82]. The

critical size for cage formation and the magic cluster $n = 16$ are also consistent with the experiments [35]. For the 4*d* transition metal yttrium, Jaiswal et al. have shown a peculiar size dependence of the structures of anionic Si_nY^- ($n = 4$–20) clusters [83]. For sizes $n = 8$, 10–15, 18, 19, the yttrium acts as a linker between two silicon sub-clusters, while for some other sizes ($n = 16$, 17, 20) the Y dopant is endohedrally encapsulated.

Besides the work on the singly doped silicon clusters, multiply doped silicon clusters recently also attracted attention. Questions of particular interest are how the additional *TM* dopants can alter the structure of the Si framework and how the local magnetic moments on the dopant atoms are coupled to one another. A PES study by Zheng and coworkers, as mentioned in Sect. 2.3, showed that $Si_{12}V^-$ has a V-centered hexagonal prism structure [38], which is slightly different from the distorted hexagonal prism of $Si_{12}V^+$ [28]. Addition of a second V dopant leads to a V capped hexagonal antiprism for $Si_{12}V_2^-$. A third V atom caps $Si_{12}V_2^-$ to form a bicapped hexagonal antiprism wheel-like structure for $Si_{12}V_3^-$. For $Si_{20}V_2^-$ those researchers predicted an elongated dodecahedron cage structure with a V_2 unit encapsulated inside the cage [84]. The strong V–V interaction makes V_2 small enough to fit into a dodecahedral Si_{20} cage. In a recent study on $Si_nV_3^-$ ($n = 3$–14) [85], a good agreement between experimental and calculated vertical and adiabatic detachment energies was found, which serves as support for the correctness of the calculated cluster geometries. They also predicted that single V doped anionic silicon clusters are encapsulated from $n = 11$ onwards.

Computationally, Khanna and coworkers studied Si_nTM_2 (*TM* = Fe, Co, Ni, Cr, and Mn; $n = 1$–8) clusters by DFT calculations [86, 87]. It was shown that these clusters display a variety of magnetic configurations with varying magnetic moment and different magnetic coupling between the two transition metal atoms depending on the cluster size and charge state. The coupling between the dopants in Si_nFe_2 and Si_nMn_2 clusters are mostly found to be ferromagnetic with large moments on the dopants, while Si_nNi_2 clusters are predicted to be nonmagnetic for most sizes. Most of Si_nCo_2 clusters have ferromagnetic ground states, but in general the magnetic moments on Co are smaller than those on the Fe and Mn dopants in silicon clusters. In cationic $Si_nCo_2^+$ ($n = 8$–12) the magnetic coupling between the Co atoms was shown to the depend on the Co–Co distance [88]. Local magnetic moments on Cr in small Si_nCr_2 ($n = 1$–5) clusters are found to be coupled ferromagnetic or anti-ferromagnetic, while larger sizes ($n = 6$–8) are nonmagnetic. Recently a non-magnetic, triple ring tubular structure with a Mn_2 dimer inside the symmetric Si skeleton was reported for $Si_{15}Mn_2$ [89]. An interesting growth pattern is found for Si_nPd_2 ($n = 10$–20) by Zhao et al. Most clusters are based on the pentagonal prism structure of $Si_{10}Pd$ [90]. In Si_nPd_2 ($n = 10$–15) one Pd dopant is located at a facial position and the other Pd dopant is inside the silicon framework, while for larger clusters ($n = 16$–20) both Pd atoms are encapsulated.

3.3 Lanthanide Dopants (kf^x $0 < x < 14$)

Lanthanide (*Ln*) doped silicon clusters are of particular interest for applications given the limited binding interaction of localized 4*f* electrons with the environment, which may imply that the lanthanide dopants maintain large magnetic moments in silicon clusters. Experimentally, lanthanide doped silicon clusters mainly have been investigated by PES. Nakajima and coworkers conducted the first study on terbium doped anionic silicon clusters, Si_nTb^- (n = 6–16) [24]. The clusters were excited using the 266 nm (4.66 eV) 4th harmonic output of a Nd:YAG laser and remarkably high electron affinities were observed for $Si_{10}Tb^-$ and $Si_{11}Tb^-$, which was interpreted as support for the onset of cage formation. The reduced reactivity of Si_nTb^- at n = 10–16 towards H_2O is further evidence that the Tb atom is located inside Si_n cages.

Bowen and coworkers investigated Si_nEu^- (n = 3–17) and revealed pronounced electronic rearrangement in the n = 10–12 size range with a remarkable increase of the electron affinities from $Si_{11}Eu^-$ (1.9 eV) to $Si_{12}Eu^-$ (2.8 eV) [37]. Such enhancement of the electron affinity is very similar to what was seen for Tb doped Si clusters before and, again, presumably reflects a geometric rearrangement due to the encapsulation of the Eu dopant atom. That one atom more is needed for cage formation in Si_nEu^- can be explained by the larger atomic radius of Eu (0.185 nm) than that of Tb (0.175 nm) and thus more silicon atoms are required to encapsulate Eu [91]. Differences between the photoelectron spectra of Si_nTb^- and Si_nEu^- were attributed to different oxidation states, Tb(III) and Eu(II), that the dopant atoms adopt in these clusters [37]. DFT calculations by Zhao et al. also predicted that, starting from n = 12, the Eu atom is located in a Si cage [92]. Interestingly, it was also found that the magnetic moments on Eu do not quench in those cages because the 4*f* electrons of the Eu atom do not interact strongly with the silicon cage. An extensive computational study of Si_nEu (n = 3–11) was recently reported by Yang et al. [93].

Bowen and coworkers later carried out a more systematic PES study to understand the electronic structures of different lanthanide dopants in silicon clusters: Si_nLn^- (n = 3–13; *Ln* = Ho, Gd, Pr, Sm, Eu, and Yb) [36]. These spectra are presented in Fig. 9. On the basis of their appearance, the *Ln* doped silicon systems can be categorized either into one of the two distinct categories A and B or in the intermediate category AB. The photoelectron spectra of Si_nEu^- and Si_nYb^- (n 12) have a common feature with a low electron binding energy and form category A. The photoelectron spectra of Ho, Gd, and Pr doped anionic Si clusters lack low energy electron binding peaks and form category B. Most interestingly, Si_nSm^- is an exception (intermediate category AB), because the small sizes $n \leq 6$ and $n = 9$ have the same low energy feature as the clusters in category A, while larger sizes $n \geq 11$ have spectra similar to the clusters in category B. Intermediate sizes of Si_nSm^- (n = 7, 8, and 10) even show features of both A and B. The different electronic features of the different lanthanide doped silicon clusters were explained by different oxidation states adopted by the lanthanide atoms. It was also claimed

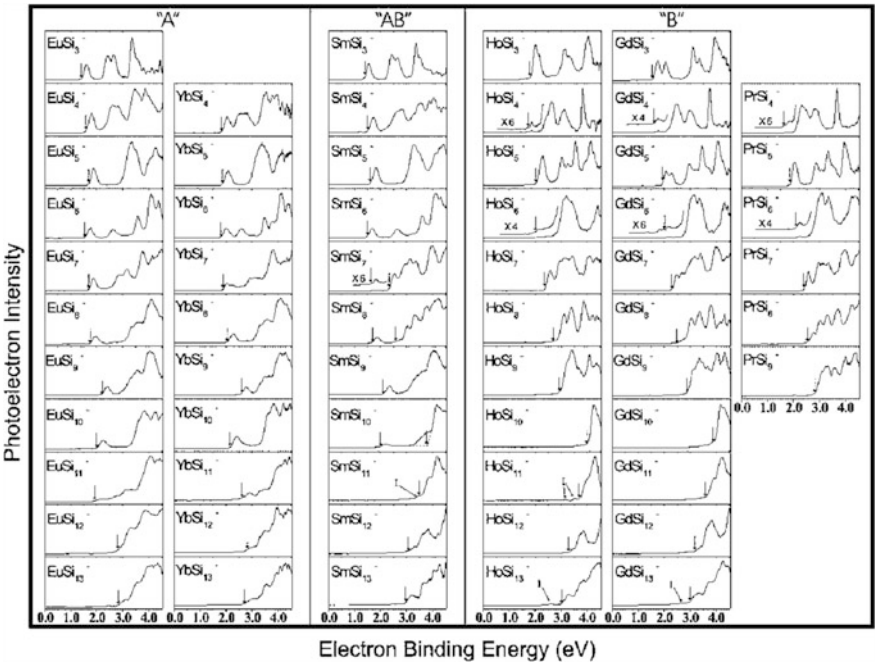

Fig. 9 Photoelectron spectra of Si_nLn^- ($3 \leq n \leq 13$) anionic clusters recorded following excitation with 266 nm photons. The *vertical arrows* indicate the threshold energies from which the adiabatic electron affinities (EA_a) of the clusters are inferred. Due to the presence of two isomers for Si_nSm^- ($n = 7, 9, 10$) two *vertical arrows* are drawn in their photoelectron spectra approximately pointing at the threshold energies of each isomer. Peaks corresponding to an impurity are marked with "*I*". The categories *A*, *B*, and *AB* are explained in the text. (Reproduced from Grubisic A et al. (2009) J Am Chem Soc 131:10783)

that based on the adopted oxidation state of the lanthanide atoms it should be possible to predict the likely electronic structures of other Si_nLn^- clusters.

Plenty of computational work has been done on lanthanide doped silicon clusters. Neutral and anionic lanthanide doped silicon clusters $Si_6Ln^{0/-}$ (*Ln* = La, Ce, Pr, Eu, Gd, Ho, Tb, Yb, and Lu) have been investigated by DFT [94–96]. It was shown that all anionic Si_6Ln^- clusters, except Si_6Yb^-, prefer structures with the *Ln* dopant atom located on top of a pentagonal bipyramid. On the other hand, in all neutral Si_6Ln clusters and in the anionic Si_6Yb^-, the dopant prefers an equatorial position in the pentagonal bipyramidal structure. In general, the magnetic moments of the dopant atoms in these clusters remain largely localized and the atomic-like magnetism is maintained in the doped clusters. Guo et al. have shown that caged lanthanide doped silicon clusters, $Si_{16}Ln$ (*Ln* = La, Ce, Pr, Nd, Sm, Eu, Gd, Tm, Yb, and Lu), favor fullerene-like over Frank-Kasper structures, which is the most stable structure for many transition metal doped clusters [97]. They found large spin magnetic moments on late lanthanide dopants (Eu: 5.85 μ_B; Gd: 6.81 μ_B), while some others (Pr, Nd, Sm, and Tm) have large orbibal moments. In addition, for

dopants in which the lanthanide 4*f* atomic orbitals are less than half-filled (Pr, Nd, and Sm) the orbital and spin moments are antiparallel to one another, but when the 4*f* atomic orbitals are more than half filled (Tm) the orbital and spin moments are parallel. Also Si_nHo (n = 1–20) has been studied computationally. Liu et al. predicted that the Ho dopant replaces a Si atom in the pure Si_{n+1} clusters for most small Si_nHo (n = 1–12) clusters with large local magnetic moments on Ho [98], while Zhao et al. suggested that the Ho dopant atom is encapsulated by a Si cage from n = 15 onwards [99]. Mulliken population analysis showed charge transfer from the Ho dopant to the Si framework for small sizes (n = 1–12), however, the calculated atomic polar tensor-based charges for larger Si_nHo (n = 12–20) indicate an inverted transfer [99]. Cao et al. found growth patterns for Si_nLu (n = 1–12) very similar to Si_nHo clusters and the calculated ground state structures of Si_nLu (n = 1–12) are formed by substituting a Si atom of the pure Si_{n+1} clusters with a Lu atom [100].

3.4 Non-metallic Main Group Dopants

Besides transition metal and lanthanide doped silicon clusters, also silicon clusters doped with main group elements have intensively been studied the last years. In this review we restrict to main group dopant elements that are not metallic in the bulk phase. In particular, Si_nX with X = B, C, O, F, N, and As will be discussed and the focus is on experimental studies.

Fielicke and coworkers obtained infrared spectra of neutral silicon carbide clusters, Si_mC_n ($m + n = 6$, $n \leq 2$), using the IR-UV2CI technique [101]. Structural assignment of Si_6, Si_5C, and Si_4C_2 was accomplished by comparison between experimental IR spectra and calculated linear absorption spectra. Computations for the entire Si_mC_n ($m + n = 6$, n = 0–6) series predict a structural transition from chain-like C_6 to three-dimensional bipyramidal structures for Si_6 (see Fig. 10). This example demonstrates that the structural differences between

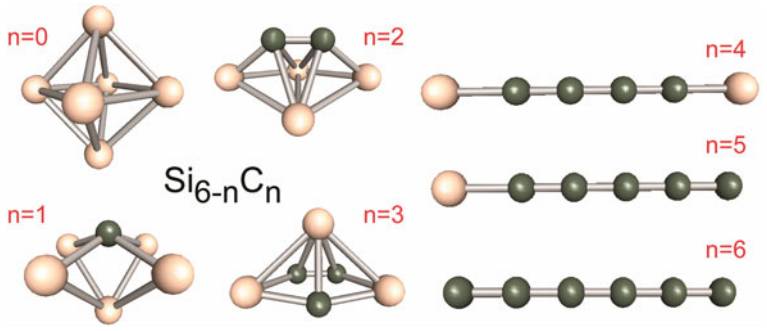

Fig. 10 Evolution of the geometrical structures of neutral $Si_{6-n}C_n$ clusters (n = 0–6). (Reproduced from Savoca M et al. (2013) J Phys Chem A 117:1158)

carbon, being flexible and exhibiting different types of sp^n (n = 1–3) hybridization, and silicon, preferring single bonds with sp^3 hybridization, are retained at the subnanometer scale. Furthermore, even for the smallest possible number of carbon atoms (n = 2), carbon segregation is observed, which can be rationalized by chemical bonding arguments. The bond strength decreases along the C–C, C–Si, Si–Si series and Si has a high ability for multicenter bonding.

Nakajima et al. investigated $Si_mC_n^-$ ($1 \leq m \leq 7$ and $1 \leq n \leq 5$) cluster anions by PES. Similar spectra were found for Si_mC^- ($3 \leq m \leq 7$) and pure Si_{m+1}^-, which was attributed to the isovalent electronic structure of Si and C atoms and suggested similar geometric structures. However, significant differences were found for SiC_n^- and C_{n+1}^- ($2 \leq n \leq 5$), which was explained by the change of the geometries [102].

Recent complementary experimental and theoretical studies dealt with the vibrational spectra and structures of neutral silicon clusters doped with first row elements Si_6X with X = Be, B, C, N, O [103, 104]. For Si_6X (X = B, C, O) calculated IR spectra could be compared to experimental spectra obtained by IR-UV2CI, while for the other clusters no experimental spectra were measured. Computations showed that the dopant atoms in Si_6X have a negative net charge and the Si atoms act as electron donors. Their structures strongly depend on the nature of the dopant atom. In particular, Be, B, and C favor structures based on the Si_7 pentagonal bipyramid with substitution at an apex, while N and O doping cause complete structural rearrangement of the silicon cluster. Also vibrational spectra of Xe-tagged cationic silicon oxide clusters $Si_nO_m^+$ with n = 3–5 and $m = n$, $n \pm 1$ have been obtained by IR-MPD [105]. For most sizes, the experimental IR spectra are consistent with the harmonic vibrational spectra of the calculated lowest energy isomer of the corresponding clusters (without considering the Xe messenger atom). In some cases ($Si_4O_3^+$, $Si_4O_5^+$, and $Si_5O_4^+$) it was found that Xe tagging changed the energetic order of the structural isomers, although the overall influence of the Xe adsorption on the cluster geometries and on the IR spectra is small. For the $Si_nO_m^+$ clusters, no simple sequential growth mechanism could be identified, but interesting structural motifs were found such as the Si_2O_2 rhombus, the Si_3O_2 pentagon, and the Si_3O_3 hexagon, which may be building blocks of larger $Si_nO_m^+$ clusters. For silicon monoxide $(SiO)_n^+$ (n = 3–5), Garand et al. used loss of a SiO unit following infrared irradiation to record action spectra [106]. Although $(SiO)_4^+$ shows a structure different from its neutral counterpart and the presence of two isomers was suggested, neutral and cationic $(SiO)_3^{+/0}$ and $(SiO)_5^{+/0}$ have similar structures.

Besides these combined experimental and computational studies, there also exist a huge number of computational studies. For instance, Avaltroni et al. studied the stability of small endohedrally B and C doped silicon clusters [107]. The atomic radius, the electronegativity and the bonding pattern of the dopant atoms were found to be the main factors that determine the relative stability of the cluster. For Si_8 it was predicted that a B dopant could stabilize a small cubic caged structure. Work by Ngan and Nguyen showed that a closed electronic shell structure, with 34 delocalized valence electrons, is able to stabilize cubic caged Si_8B^+, Si_8Be, and

Si_8C^{2+} isomers [16]. They found that the Si atoms in the cluster have sp^3 hydridization and that dangling bonds are saturated by the main group dopant atoms. Later studies of the same group identified the growth mechanism of boron doped silicon clusters Si_nB (n = 1–10) [108]. They found that Si_nB can be formed by adding a Si atom to $Si_{n-1}B$ and the B dopant is encapsulated by a Si_n cage from n = 8 onwards, although the predicted lowest energy isomer of Si_8B is based on a pentagonal bipyramidal motif and is not a cube. The high stability of Si_9B^- and $Si_{10}B^+$ is claimed to originate from closed electronic shells and from spherical aromaticity. For C doped silicon clusters, a planar tetracoordinated carbon Si_4C^{2+} structure with enhanced stability was predicted, which is a building block for Si_9C [109]. Combined effects of the electron delocalization and geometrical constraint of the Si_9 and an additional electrostatic interaction also contribute to the cluster stabilization.

Also fluorine has been considered as dopant in silicon clusters. Zhang et al. conducted a systematical study of the geometries, stabilities, and electronic properties of Si_nF (n = 1–12) by first-principles calculations [110]. The located ground state structures of Si_nF (n = 1–12) are all exohedral and the F dopant was found to enhance the chemical reactivity and to reduce the stability of the pure Si clusters with smaller HOMO–LUMO gaps in the F doped clusters compared to the corresponding pure silicon clusters. They also found negative charges on the F dopant for the studied sizes. Arsenic doped silicon clusters, Si_nAs (n = 1–14), have been studied by Kodlaa et al. [111]. The As dopant seems to have a limited effect on the structures of the pure Si clusters and favors to adsorb to the pure Si_n clusters at exohedral positions. Interestingly, enhanced metallic characteristics were found for the larger clusters, i.e., from n = 4 onwards.

4 Summary and Outlook

In this chapter, we presented a review of recent progress on the structural identification of doped silicon clusters. Besides geometric structures, also electronic and magnetic properties of the clusters are briefly commented on. Growth patterns of the doped silicon clusters are discussed and clusters with appealing structural, electronic, or magnetic properties are identified. As dopant elements coinage metals, transition metals, lanthanides, and non-metallic main-group atoms were considered. Experimentally, the main techniques that have been applied in recent years for studying doped silicon clusters in the gas phase are chemical probe mass spectrometry methods, IR action spectroscopy, photoelectron spectroscopy, and x-ray absorption spectroscopy. Computationally most work makes use of the density functional theory formalism.

Specific doped silicon clusters with appealing properties may be used in future applications. However, it is important to realize that the current chapter dealt with isolated clusters in the gas phase. In devices, the interactions with the environment will affect the cluster's properties. Further extension of the work should deal with

deposited size selected clusters, which have potential as building blocks of nano-assemblies in microelectronic devices. The choice of the substrate will be crucial, as the geometric and electronic properties of these clusters will be altered by interaction with the support. Recently, using scanning tunneling microscopy (STM), Nakajima and coworkers investigated the initial products created by the deposition of gas phase synthesized $Si_{16}Ta^+$, which is predicted to be very stable, on monolayer films of C_{60} molecules. $Si_{16}Ta–C_{60}$ heterodimers are formed preferentially [112]. They also demonstrated that densely packed $Si_{16}Ta^+$ clusters can be immobilized onto C_{60} terminated surfaces, while retaining their cage shape and positive charge [113]. Another example concerns materials based on $Si_{12}V^+$. Its symmetric hexagonal prism structure in the gas phase [28] inspired researchers to build networks with $Si_{12}V^+$ as building block. A first-principle calculation demonstrated that hexagonal porous and honeycomb-like frameworks build up from $Si_{12}V$ units with regularly and separately distributed V atoms are stable at room temperature [114]. The preferred magnetic coupling in both the hexagonal porous and honeycomb-like sheets is found to be ferromagnetic due to a free-electron-mediated mechanism. By using external strain, it was shown that the magnetic moments and the strength of the magnetic coupling with the sheets can be deliberately tuned [115], which is propitious for advanced applications, in particular for 2D silicon-based spintronic nanomaterials.

Another subject that needs further exploration is multiply doped silicon clusters, especially using magnetic dopants. In these systems, the magnetic coupling between the dopant atoms can be tuned by the size of the silicon host cage and by the interaction with the silicon which can be strongly size-dependent [38, 86, 87]. This approach could allow to control the magnetic properties in silicon clusters.

Acknowledgments We gratefully acknowledge all who contributed to our original papers on the structural identification of doped silicon clusters: Pieterjan Claes, Philipp Gruene, Marko Haertelt, Dan J. Harding, Jonathan T. Lyon, Gerard Meijer, Vu Thi Ngan, Minh Tho Nguyen, Nguyen Minh Tam, Alex Woodham, and Ludger Wöste. The authors are thankful to the Stichting voor Fundamenteel Onderzoek der Materie (FOM) in providing beam time on FELIX and highly appreciate the skillful assistance of the FELIX staff. This work is supported by the Research Foundation-Flanders (FWO), the KU Leuven Research Council (GOA 14/007), and the Deutsche Forschungsgemeinschaft within FOR 1282 (FI 893/4).

References

1. Bloomfield LA, Freeman RR, Brown WL (1985) Photofragmentation of mass-resolved $Si_{2\text{-}12}^+$ clusters. Phys Rev Lett 54:2246–2249
2. Heath JR, Liu Y, O'Brien SC, Zhang QL, Curl RF, Tittel FK, Smalley RE (1985) Semiconductor cluster beams—one and two color ionization studies of Si_x and Ge_x. J Chem Phys 83:5520–5526
3. Martin TP, Schaber H (1985) Mass spectra of Si, Ge, and Sn clusters. J Chem Phys 83:855–858

4. Shvartsburg AA, Hudgins RR, Dugourd P, Jarrold MF (2001) Structural information from ion mobility measurements: applications to semiconductor clusters. Chem Soc Rev 30:26–35
5. Zhang QL, Liu Y, Curl RF, Tittel FK, Smalley RE (1987) Photodissociation of semiconductor positive cluster ions. J Chem Phys 88:1670–1677
6. Rothlisberger U, Andreoni W, Parrinello M (1994) Structure of nanoscale silicon clusters. Phys Rev Lett 72:665–668
7. Veldeman N, Gruene P, Fielicke A, Ngan VT, Nguyen MT, Lievens P (2010) Endohedrally doped silicon clusters. In: Sattler KD (ed) Handbook of nanophysics: clusters and fullerenes. CRC Press Boca Raton
8. Kumar V (2007) Metal encapsulated clusters of silicon: silicon fullerenes and other polyhedral forms. In: Kumar V (ed) Nanosilicon. Elsevier London, pp 114–148
9. Jackson K, Nellermoe B (1996) $Zr@Si_{20}$: a strongly bound Si endohedral system. Chem Phys Lett 254:249
10. Hiura H, Miyazaki T, Kanayama T (2001) Formation of metal-encapsulating Si cage clusters. Phys Rev Lett 86:1733–1736
11. Kumar V, Kawazoe Y (2001) Metal-encapsulated fullerenelike and cubic caged clusters of silicon. Phys Rev Lett 87:045503
12. Reveles JU, Khanna SN (2006) Electronic counting rules for the stability of metal-silicon clusters. Phys Rev B 74:035435
13. Koyasu K, Akutsu M, Mitsui M, Nakajima A (2005) Selective formation of MSi_{16} (M = Sc, Ti, and V). J Am Chem Soc 127:4998–4999
14. Beck SM (1987) Studies of silicon cluster–metal atom compound formation in a supersonic molecular beam. J Chem Phys 87:4233–4234
15. Khanna SN, Rao BK, Jena P (2002) Magic numbers in metallo-inorganic clusters: chromium encapsulated in silicon cages. Phys Rev Lett 89:016803
16. Ngan VT, Nguyen MT (2010) The aromatic 8-electron cubic silicon clusters $Be@Si_8$, $B@Si_8^+$ and $C@Si_8^{2+}$. J Phys Chem A 114:7609–7615
17. Fielicke A, Lyon JT, Haertelt M, Meijer G, Claes P, de Haeck J, Lievens P (2009) Vibrational spectroscopy of neutral silicon clusters via far-IR-VUV two color ionization. J Chem Phys 131:171105
18. Raghavachari K (1986) Theoretical study of small silicon clusters: Equilibrium geometries and electronic structures of $Si_{2\text{-}7}$, Si_{10}. J Chem Phys 84:5672–5686
19. Zdetsis AD (2007) Fluxional and aromatic behavior in small magic silicon clusters: a full ab initio study of Si_n, Si_n^{1-}, Si_n^{2-}, and Si_n^{1+}, n = 6, 10 clusters. J Chem Phys 127:014314
20. Lyon JT, Gruene P, Fielicke A, Meijer G, Janssens E, Claes P, Lievens P (2009) Structures of silicon cluster cations in the gas phase. J Am Chem Soc 131:1115–1121
21. Chauhan V, Abreu MB, Reber AC, Khanna SN (2015) Geometry controls the stability of $FeSi_{14}$. Phys Chem Chem Phys 17:15718–15724
22. Phi DN, Trung NT, Janssens E, Ngan VT (2016) Electron counting rules for transition metal-doped Si_{12} clusters. Chem Phys Lett 643:103–108
23. Torres MB, Fernández EM, Balbás LC (2007) Theoretical study of isoelectronic Si_nM clusters (M = Sc^-, Ti, V^+; n = 14–18). Phys Rev B 75:205425
24. Ohara M, Miyajima K, Pramann A, Nakajima A, Kaya K (2002) Geometric and electronic structures of terbium-silicon mixed clusters ($TbSi_n$; $6 \leq n \leq 16$). J Phys Chem A 106:3702–3705
25. Janssens E, Gruene P, Meijer G, Wöste L, Lievens P, Fielicke A (2007) Argon physisorption as a structural probe for endohedral doped silicon clusters. Phys Rev Lett 99:063401
26. Zamudio-Bayer V, Leppert L, Hirsch K, Langenberg A, Rittmann J, Kossick M, Vogel M, Richter R, Terasaki A, Möller T, von Issendorff B, Kummel S, Lau JT (2013) Coordination-driven magnetic-to-nonmagnetic transition in manganese-doped silicon clusters. Phys Rev B 88:115425
27. Asmis KR, Fielicke A, von Helden G, Meijer G. Vibrational spectroscopy of gas-phase clusters and complexes. In: Woodruff DP (ed) Atomic cluster: from gas phase to deposited. Elsevier, Amsterdam

28. Claes P, Janssens E, Ngan VT, Gruene P, Lyon JT, Harding DJ, Fielicke A, Nguyen MT, Lievens P (2011) Structural identification of caged vanadium doped silicon clusters. Phys Rev Lett 107:173401
29. Claes P, Ngan VT, Haertelt M, Lyon JT, Fielicke A, Nguyen MT, Lievens P, Janssens E (2013) The structures of neutral transition metal doped silicon clusters, Si_nX (n = 6–9; X = V, Mn). J Chem Phys 138:194301
30. Li Y, Lyon JT, Woodham AP, Fielicke A, Janssens E (2014) The geometric structure of silver-doped silicon clusters. ChemPhysChem 15:328–336
31. Li Y, Lyon JT, Woodham AP, Lievens P, Fielicke A, Janssens E (2015) Structural identification of gold doped silicon clusters via far-infrared spectroscopy. J Phys Chem C 119:10896–10903
32. Ngan VT, Janssens E, Claes P, Lyon JT, Fielicke A, Nguyen MT, Lievens P (2012) High magnetic moments in manganese-doped silicon clusters. Chem Eur J 18:15788–15793
33. Ngan VT, Gruene P, Claes P, Janssens E, Fielicke A, Nguyen MT, Lievens P (2010) Disparate effects of Cu and V on structures of exohedral transition metal-doped silicon clusters: A combined far-infrared spectroscopic and computational study. J Am Chem Soc 132:15589–15602
34. Koyasu K, Atobe J, Akutsu M, Mitsui M, Nakajima A (2007) Electronic and geometric stabilities of clusters with transition metal encapsulated by silicon. J Phys Chem A 111:42–49
35. Ohara M, Koyasu K, Nakajima A, Kaya K (2003) Geometric and electronic structures of metal (M)-doped silicon clusters (M = Ti, Hf, Mo and W). Chem Phys Lett 371:490–497
36. Grubisic A, Ko YJ, Wang H, Bowen KH (2009) Photoelectron spectroscopy of lanthanide-silicon cluster anions $LnSi_n^-$ ($3 \leq n \leq 13$; Ln = Ho, Gd, Pr, Sm, Eu, Yb): Prospect for magnetic silicon-based clusters. J Am Chem Soc 131:10783–10790
37. Grubisic A, Wang H, Ko YJ, Bowen KH (2008) Photoelectron spectroscopy of europium-silicon cluster anions, $EuSi_n^-$ ($3 \leq n \leq 17$). J Chem Phys 129:054302
38. Huang X, Xu HG, Lu S, Su Y, King RB, Zhao J, Zheng W (2014) Discovery of a silicon-based ferromagnetic wheel structure in $V_xSi_{12}^-$ (x = 1–3) clusters: Photoelectron spectroscopy and density functional theory investigation. Nanoscale 6:14617
39. Kong X, Xu HG, Zheng W (2012) Structures and magnetic properties of $CrSi_n^-$ (n = 3–12) clusters: photoelectron spectroscopy and density functional calculations. J Chem Phys 137:064307
40. Kong XY, Deng XJ, Xu HG, Yang Z, Xu XL, Zheng W (2013) Photoelectron spectroscopy and density functional calculations of $AgSi_n^-$ (n = 3–12) clusters. J Chem Phys 138:244312
41. Tai TB, Nguyen MT (2012) Electronic structure and thermochemical properties of silicon-doped lithium clusters $Li_nSi^{0/+}$, n = 1–8: new insights on their stability. J Comp Chem 33:800–809
42. Tam NM, Tai TB, Ngan VT, Nguyen MT (2013) Structure, thermochemical properties, and growth sequence of aluminum-doped silicon clusters Si_nAl_m (n = 1–11, m = 1–2) and their anions. J Phys Chem A 117:6867–6882
43. Majumder C, Kulshreshtha SK (2004) Influence of Al substitution on the atomic and electronic structure of Si clusters by density functional theory and molecular dynamics simulations. Phys Rev B 69:115432
44. Nigam S, Majumder C, Kulshreshtha SK (2006) Structural and electronic properties of Si_n, Si_n^-, and PSi_{n-1} clusters ($2 \leq n \leq 13$): theoretical investigation based on ab initio molecular orbital theory. J Chem Phys 125:074303
45. Rabilloud F, Sporea C (2007) Ab initio investigation of structures and properties of mixed silicon-potassium Si_nK_p and $Si_nK_p^+$ ($n \leq 6$, $p \leq 2$) clusters. J Comput Methods Sci Eng 7:273–286
46. Sporea C, Rabilloud F, Aubert-Frécon M (2007) Charge transfers in mixed silicon–alkali clusters and dipole moments. J Mol Struc-Theochem 802:85–90

47. Sporea C, Rabilloud F, Cosson X, Allouche AR, Aubert-Frécon M (2006) Theoretical study of mixed silicon—lithium clusters $Si_nLi_p^{(+)}$ (n = 1–6, p = 1–2). J Phys Chem A 110:6032–6038
48. De Haeck J, Bhattacharyya S, Le HT, Debruyne D, Tam NM, Ngan VT, Janssens E, Nguyen MT, Lievens P (2012) Ionization energies and structures of lithium doped silicon clusters. Phys Chem Chem Phys 14:8542–8550
49. Neukermans S, Wang X, Veldeman N, Janssens E, Silverans RE, Lievens P (2006) Mass spectrometric stability study of binary MS_n clusters (S = Si, Ge, Sn, Pb, and M = Cr, Mn, Cu, Zn). Int J Mass Spectrom 252:145–150
50. Koyasu K, Atobe J, Furuse S, Nakajima A (2008) Anion photoelectron spectroscopy of transition metal- and lanthanide metal-silicon clusters: MSi_n^- (n = 6–20). J Chem Phys 129:214301
51. Ngan VT, Janssens E, Claes P, Fielicke A, Nguyen MT, Lievens P (2015) Nature of the interaction between rare gas atoms and transition metal doped silicon clusters: the role of shielding effects. Phys Chem Chem Phys 17:17584–17591
52. Andriotis AN, Mpourmpakis G, Froudakis GE, Menon M (2002) Stabilization of Si-based cage clusters and nanotubes by encapsulation of transition metal atoms. New J Phys 4:78
53. Menon M, Andriotis AN, Froudakis GE (2002) Structure and stability of Ni-encapsulated Si nanotube. Nano Lett 2:301–304
54. Asmis KR (2012) Structure characterization of metal oxide clusters by vibrational spectroscopy: possibilities and prospects. Phys Chem Chem Phys 14:9270–9281
55. http://www.ru.nl/felix/
56. Raghavachari K, Logovinsky V (1985) Structure and bonding in small silicon clusters. Phys Rev Lett 55:2853
57. Okumura M, Yeh LI, Lee YT (1985) The vibrational predissociation spectroscopy of hydrogen clusters ions. J Chem Phys 83:3705
58. Okumura M, Yeh LI, Myers JK, Lee YT (1986) Infrared spectra of the cluster ions $H_7O_3^+ \cdot H_2$ and $H_9O_4^+ \cdot H_2$. J Chem Phys 85:2328
59. Savoca M, Langer J, Harding DJ, Dopfer O, Fielicke A (2013) Incipient chemical bond formation of Xe to a cationic silicon cluster: vibrational spectroscopy and structure of the Si_4Xe^+ complex. Chem Phys Lett 557:49–52
60. Calvo F, Li Y, Kiawi DM, Bakker JM, Parneix P, Janssens E (2015) Nonlinear effects in infrared action spectroscopy of silicon and vanadium oxide clusters: experiment and kinetic modeling. Phys Chem Chem Phys 17:25956–25967
61. Li Y, Tam NM, Claes P, Woodham AP, Lyon JT, Ngan VT, Nguyen MT, Lievens P, Fielicke A, Janssens E (2014) Structure assignment, electronic properties, and magnetism quenching of endohedrally doped neutral silicon clusters, Si_nCo (n = 10–12). J Phys Chem A 118:8198–8203
62. Hirsch K, Lau JT, Klar Ph, Langenberg A, Probst J, Rittmann J, Vogel M, Zamudio-Bayer V, Möller T, von Issendorff B (2009) X-ray spectroscopy on size-selected clusters in an ion trap: from the molecular limit to bulk properties. J Phys B: At Mol Opt Phys 42:154029
63. Peredkov S, Neeb M, Eberhardt W, Meyer J, Tombers M, Kampschulte H, Niedner-Schatteburg G (2011) Spin and orbital magnetic moments of free nanoparticles. Phys Rev Lett 107:233401
64. Lau JT, Hirsch K, Klar Ph, Langenberg A, Lofink F, Richter R, Rittmann J, Vogel M, Zamudio-Bayer V, Möller T, von Issendorff B (2009) X-ray spectroscopy reveals high symmetry and electronic shell structure of transition-metal-doped silicon clusters. Phys Rev A 79:053201
65. Lau JT, Vogel M, Langenberg A, Hirsch K, Rittmann J, Zamudio-Bayer V, Möller T, von Issendorff B (2011) Highest occupied molecular orbital–lowest unoccupied molecular orbital gaps of doped silicon clusters from core level spectroscopy. J Chem Phys 134:041102
66. Xiao C, Hagelberg F (2002) Geometric, energetic, and bonding properties of neutral and charged copper-doped silicon clusters. Phys Rev B 66:075425

67. Chuang FC, Hsieh YY, Hsu CC, Albao MA (2007) Geometries and stabilities of Ag-doped Si_n (n = 1-13) clusters: a first-principles study. J Chem Phys 127:144313
68. Ziella DH, Caputo MC, Provasi P (2010) Study of geometries and electronic properties of $AgSi_n$ cluster using DFT/TB. Int Quantum Chem 111:1680–1693
69. Wang J, Liu Y, Li YC (2010) Au@Sin: growth behavior, stability and electronic structure. Phys Lett A 374:2736–2742
70. Chuang FC, Hsu CC, Hsieh YY, Albao MA (2010) Atomic and electronic structures of $AuSi_n$ (n = 1–16) clusters: a first-principles study. Chin J Phys 48:82–102
71. Gruene P, Fielicke A, Meijer M, Janssens E, Ngan VT, Nguyen MT, Lievens P (2008) Tuning the geometric structure by doping silicon clusters. ChemPhysChem 9:703–706
72. Hagelberg F, Xiao C, Lester WA (2003) Cagelike Si_{12} clusters with endohedral Cu, Mo, and W metal atom impurities. Phys Rev B 67:035426
73. Guo LJ, Zhao GF, Gu YZ, Liu X, Zeng Z (2008) Density-functional investigation of metal-silicon cage clusters MSin (M = Sc, Ti, V, Cr, Mn, Fe Co, Ni, Cu, Zn; n = 8–16). Phys Rev B 77:195417
74. Ma L, Zhao JJ, Wang JG, Wang BL, Lu QL, Wang GH (2006) Growth behavior and magnetic properties of Si_nFe (n = 2–17) cluster. Phys Rev B 73:125439
75. Xu HG, Wu MM, Zhang ZG, Yuan J, Sun Q, Zheng W (2012) Photoelectron spectroscopy and density functional calculations of $CuSi_n^-$ (n = 4–18) Clusters. J Chem Phys 136:104308
76. Palagin D, Gramzow M, Reuter K (2011) On the stability of "non-magic" endohedrally doped Si clusters: a first-principles sampling study of MSi_{16}^+ (M = Ti, V, Cr). J Chem Phys 134:244705
77. Reveles JU, Khanna SN (2005) Nearly-free-electron gas in a silicon cage. Phys Rev B 72:165413
78. Zheng W, Nilles JM, Radisic D, Bowen KH (2005) Photoelectron spectroscopy of chromium-doped silicon cluster anions. J Chem Phys 122:071101
79. Xu HG, Zhang ZG, Feng Y, Yuan J, Zhao Y, Zheng W (2010) Vanadium-doped small silicon clusters: photoelectron spectroscopy and density-functional calculations. Chem Phys Lett 487:204–208
80. Liu Y, Li GL, Gao AM, Chen HY, Finlow D, Li QS (2011) The structures and properties of $FeSi_n/FeSi_n^+/FeSi_n^-$ (n = 1–8) clusters. Eur Phys J D 64:27–35
81. Deng C, Zhou L, Li G, Chen H, Li Q (2012) Theoretical studies on the structures and stabilities of charged, titanium-doped, small silicon clusters, $TiSi_n^-/TiSi_n^+$ (n = 1–8). J Clust Sci 23:975–993
82. Kawamura H, Kumar V, Kawazoe Y (2005) Growth behavior of metal-doped silicon clusters Si_nM (M = Ti, Zr, Hf; n = 8–16). Phys Rev B 71:075423
83. Jaiswal S, Babar VP, Kumar V (2013) Growth behavior, electronic structure, and vibrational properties of Si_nY anion clusters (n = 4–20): Metal atom as linker and endohedral dopant. Phys Rev B 88:085412
84. Xu HG, Kong XY, Deng XJ, Zhang ZG, Zheng W (2014) Smallest fullerene-like silicon cage stabilized by a V_2 unit. J Chem Phys 140:024308
85. Huang X, Xu HG, Lu S, Su Y, King RB, Zhao J, Zheng W (2014) Discovery of a silicon-based ferromagnetic wheel structure in $V_xSi_{12}^-$ (x = 1–3) clusters: photoelectron spectroscopy and density functional theory investigation. Nanoscale 6:14617
86. Robles R, Khanna SN, Castleman AW (2008) Stability and magnetic properties of T_2Si_n (T = Cr, Mn, $1 \leq n \leq 8$) clusters. Phys Rev B 77:235441
87. Robles R, Khanna SN (2009) Stable T_2Si_n (T = Fe Co, Ni, $1 \leq n \leq 8$) cluster motifs. J Chem Phys 130:164313
88. Li Y, Tam NM, Woodham AP, Lyon JT, Li Z, Lievens P, Fielicke A, Nguyen MT, Janssens E (2016) Structure dependent magnetic coupling in cobalt-doped silicon clusters. J Phys Chem C 120:19454–19460
89. Pham HT, Phan TT, Tam NM, Van Duong L, Pham-Ho MP, Nguyen MT (2015) $Mn_2@Si_{15}$: the smallest triple ring tubular silicon cluster. Phys Chem Chem Phys 17:17566–17570

90. Zhao RN, Han JG, Duan Y (2014) Density Functional theory investigations on the geometrical and electronic properties and growth patterns of Si_n (n = 10–20) clusters with bimetal Pd_2 impurities. Thin Solid Films 556:571–579
91. WebElements periodic table. http://www.webelements.com/
92. Zhao G, Sun J, Gu Y, Wang Y (2009) Density-functional study of structural, electronic, and magnetic properties of the Si_nEu (n = 1–13) clusters. J Chem Phys 131:114312
93. Yang J, Wang J, Hao Y (2015) Europium-doped silicon clusters $EuSi_n$ (n = 3–11) and their anions: structures, thermochemistry, electron affinities, and magnetic moments. Theo Chem Acc 134:81
94. Li HF, Kuang XY, Wang HQ (2011) Probing the structural and electronic properties of lanthanide-metal-doped silicon clusters: $M@Si_6$ (M = Pr, Gd, Ho). Phys Lett A 375:2836–2844
95. Wang HQ, Li HF (2014) A combined stochastic search and density functional theory study on the neutral and charged silicon-based clusters MSi_6 (M = La, Ce, Yb and Lu). RSC Adv 4:29782–29793
96. Xu W, J WX, Xiao Y, Wang SG (2015) Stable structures of $LnSi_6$—and $LnSi_6$ clusters (Ln = Pr, Eu, Gd, Tb, Yb), C_{2v} or C_{5v}? Explanation of photoelectron spectra. Comp Theo Chem 1070: 1–8
97. Guo L, Zheng X, Zeng Z, Zhang C (2012) Spin orbital effect in lanthanides doped silicon cage clusters. Chem Phys Lett 550:134–137
98. Liu TG, Zhang WQ, Li YL (2013) First-principles study on the structure, electronic and magnetic properties of $HoSi_n$ (n = 1–12, 20) clusters. Front Phys 9:210–218
99. Zhao RN, Han JG (2014) Geometrical stabilities and electronic properties of Si_n (n = 12–20) clusters with rare earth holmium impurity: a density functional investigation. RSC Adv 4:64410–64418
100. Cao TT, Zhao LX, Feng XJ, Lei YM, Luo YH (2008) Structural and electronic properties of $LuSi_n$ (n = 1–12) clusters: A density functional theory investigation. J Mol Struc-Theochem 895:148–155
101. Savoca M, Lagutschenkov A, Langer J, Harding DJ, Fielicke A (2013) Vibrational spectra and structures of neutral Si_mC_n clusters ($m + n$ = 6): sequential doping of silicon clusters with carbon atoms. J Phys Chem A 117:1158–1163
102. Nakajima A, Taguwa T, Nakao K, Gomei M, Kishi R, Iwata S, Kaya K (1995) Photoelectron spectroscopy of silicon–carbon cluster anions ($Si_nC_m^-$). J Chem Phys 103:2050–2057
103. Truong NX, Savoca M, Harding DJ, Fielicke A, Dopfer O (2014) Vibrational spectra and structures of neutral Si_6X clusters (X = Be, B, C, N, O). Phys Chem Chem Phys 16:22364–22372
104. Truong NX, Haertelt M, Jaeger BKA, Gewinner S, Schöllkopf W, Fielicke A, Dopfer O (2016) Characterization of neutral boron-silicon clusters using infrared spectroscopy: the case of Si_6B. Int J Mass Spectrom 395:1–6
105. Savoca M, Langer J, Harding DJ, Palagin D, Reuter K, Dopfer O, Fielicke A (2014) Vibrational spectra and structures of bare and Xe-tagged cationic $Si_nO_m^+$ clusters. J Chem Phys 141:104313
106. Garand E, Goebbert D, Santambrogio G, Janssens E, Lievens P, Meijer G, Neumark DM, Asmis KR (2008) Vibrational spectra of small silicon monoxide cluster cations measured by infrared multiple photon dissociation spectroscopy. Phys Chem Chem Phys 10:1502–1506
107. Avaltroni F, Steinmann SN, Corminboeuf C (2012) How are small endohedral silicon clusters stabilized? Phys Chem Chem Phys 14:14842–14849
108. Tam NM, Tai TB, Nguyen MT (2012) Thermochemical parameters and growth mechanism of the boron-doped silicon clusters, Si_nB^q with n = 1–10 and q = −1, 0, +1. J Phys Chem C 116:20086–20098
109. Tam NM, Ngan VT, Nguyen MT (2013) Planar tetracoordinate carbon stabilized by heavier congener cages: the Si_9C and Ge_9C clusters. Chem Phys Lett 595–596:272–276

110. Zhang S, Jiang HL, Wang P, Lu C, Li GQ, Zhang P (2013) Structures, stabilities, and electronic properties of F-doped Si_n (n = 1–12) clusters: Density functional theory investigation. Chin Phys B 22:123601
111. Kodlaa A, El-Taher S (2012) A DFT study on the structures and stabilities of As-doped Si_{n-1} (n = 2–15) clusters. Comp Theo Chem 992:134–141
112. Nakaya M, Nakaya M, Iwasa T, Tsunoyama H, Eguchi T, Nakajima A (2015) Heterodimerization via the covalent bonding of $Ta@Si_{16}$ nanoclusters and C_{60} molecules. J Phys Chem C 119:10962–10968
113. Nakaya M, Iwasa T, Tsunoyama H, Eguchi T, Nakajima A (2014) Formation of a superatom monolayer using gas-phase-synthesized $Ta@Si_{16}$ nanocluster ions. Nanoscale 6:14702–14707
114. Liu Z, Wang X, Cai J, Zhu H (2015) Room-temperature ordered spin structures in cluster-assembled single $V@Si_{12}$ sheets. J Phys Chem C 119:1517–1523

http://www.springer.com/978-3-319-48916-2

Clusters
Structure, Bonding and Reactivity
Nguyen, M.T.; Kiran, B. (Eds.)
2017, XII, 363 p. 161 illus., Hardcover
ISBN: 978-3-319-48916-2